DEVELOPMENTAL BIOLOGY

eIF4A2 targets developmental potency and histone H3.3 transcripts for translational control of stem cell pluripotency

Dan Li[1,2,3], Jihong Yang[1], Xin Huang[1], Hongwei Zhou[1], Jianlong Wang[1]*

Translational control has emerged as a fundamental regulatory layer of proteome complexity that governs cellular identity and functions. As initiation is the rate-limiting step of translation, we carried out an RNA interference screen for key translation initiation factors required to maintain embryonic stem cell (ESC) identity. We identified eukaryotic translation initiation factor 4A2 (eIF4A2) and defined its mechanistic action through ribosomal protein S26–independent and –dependent ribosomes in translation initiation activation of messenger RNAs (mRNAs) encoding pluripotency factors and the histone variant H3.3 with demonstrated roles in maintaining stem cell pluripotency. eIF4A2 also mediates translation initiation activation of Ddx6, which acts together with eIF4A2 to restrict the totipotent two-cell transcription program in ESCs through Zscan4 mRNA degradation and translation repression. Accordingly, knockdown of eIF4A2 disrupts ESC proteome, causing the loss of ESC identity. Collectively, we establish a translational paradigm of the protein synthesis of pluripotency transcription factors and epigenetic regulators imposed on their established roles in controlling pluripotency.

INTRODUCTION

Cellular identity is driven by widespread gene expression control in multiple regulatory layers, with heterogeneity in the cellular epigenome, transcriptome, and proteome. Although initial work focused on dissecting the transcriptome and epigenome in safeguarding stem cell identity (*1*), RNA expression cannot directly determine protein abundance and cellular identity. Increasing studies have revealed the importance of posttranscriptional control in embryonic stem cells (ESCs) (*2*), and mRNA translation ranked first among all the enriched biological processes in analyzing the genes necessary for ESC maintenance (*3*). In ESCs, protein abundance and chromatin landscapes are susceptible to the alternations of translational control (*4*). However, mechanisms of mRNA translational control, particularly the rate-limiting translation initiation control in safeguarding ESC identity, remain poorly defined.

Mouse ESCs do not usually differentiate into extraembryonic trophoblast lineage, except for a minor population of bipotential two-cell (2C)–like cells with both embryonic and extraembryonic differentiation propensities (*5*). While genetic manipulation of transcription programs and epigenetic machinery (*6*–*8*) can overcome this barrier, it is currently unknown whether a translational control mechanism exists to restrict the totipotent 2C program and extraembryonic lineage propensity in maintaining pluripotency.

Starting from an RNA interference (RNAi) screen to identify key translation initiation factors (TIFs) that are required for maintaining ESC identity, we found in this study that eukaryotic TIF 4A2 (eIF4A2) mediates a unique translation program by acting as both a translation activator and a repressor to control the expression of cellular potency regulators, including pluripotency factors and totipotency regulators, and epigenetic regulators, including a specific histone variant and a polycomb protein, which shapes the proteome of ESCs in safeguarding pluripotent stem cell identity.

RESULTS

An RNAi screen identifies eIF4A2 as a critical TIF for ESC maintenance

TIFs include eIFs and other factors involved in translation initiation (*9*) (Fig. 1A). While TIF RNA expression is dynamically regulated during mouse early embryogenesis, most TIF proteins are uniformly up-regulated to the highest level at the blastocyst stage (fig. S1A) (*10*), from which ESCs can be derived, suggesting a potentially profound translation initiation control in ESCs.

To explore the functional significance of TIFs in regulating ESC identity, we performed an RNAi screen with three independent and constitutive short hairpin RNAs (shRNAs; sh1 to sh3 in Fig. 1C) targeting all 68 TIFs for ESC maintenance (Fig. 1, B and C). The screen was repeated once with high reproducibility (the two columns in Fig. 1C) and resulted in various ESC statuses ranging from undifferentiated (red; sh*GFP*/sh*eIF4G2* as control/hit example) to moderately differentiated (pink; sh*Nanog*/sh*eIF4H* as control/hit example) to fully differentiated (gray; sh*Sox2*/sh*eIF4A2* as control/hit example) cell states (Fig. 1, C and D). Candidate hits that resulted in cell death/loss were scored as "too few colonies" (white) (Fig. 1C). We found that knockdown (KD) of the TIFs previously reported for ESC maintenance (*3*, *11*), such as eIF2B3 and eIF2S2, also showed moderate differentiation (Fig. 1C) and that depletion of eIF4G2 [also known as novel APOBEC1 target 1 (Nat1)] maintains, or even slightly enhances, typical dome-shaped and alkaline phosphatase (AP)–positive ESC morphology as reported (Fig. 1, C and D) (*12*), supporting the validity of our screen. Overall, our screen of 68 TIFs identified 10 TIFs (Fig. 1C, highlighted in yellow) whose depletion induced severe differentiation and/or death in ESCs. To identify TIFs specifically required for ESC pluripotency instead of cellular viability,

[1]Department of Medicine, Columbia Center for Human Development, Columbia Stem Cell Initiative, Herbert Irving Comprehensive Cancer Center, Columbia University Irving Medical Center, New York, NY 10032, USA. [2]Department of Cell, Developmental, and Regenerative Biology, Black Family Stem Cell Institute, Icahn School of Medicine at Mount Sinai, New York, NY 10029, USA. [3]Graduate School of Biomedical Sciences, Icahn School of Medicine at Mount Sinai, New York, NY 10029, USA.
*Corresponding author. Email: jw3925@cumc.columbia.edu

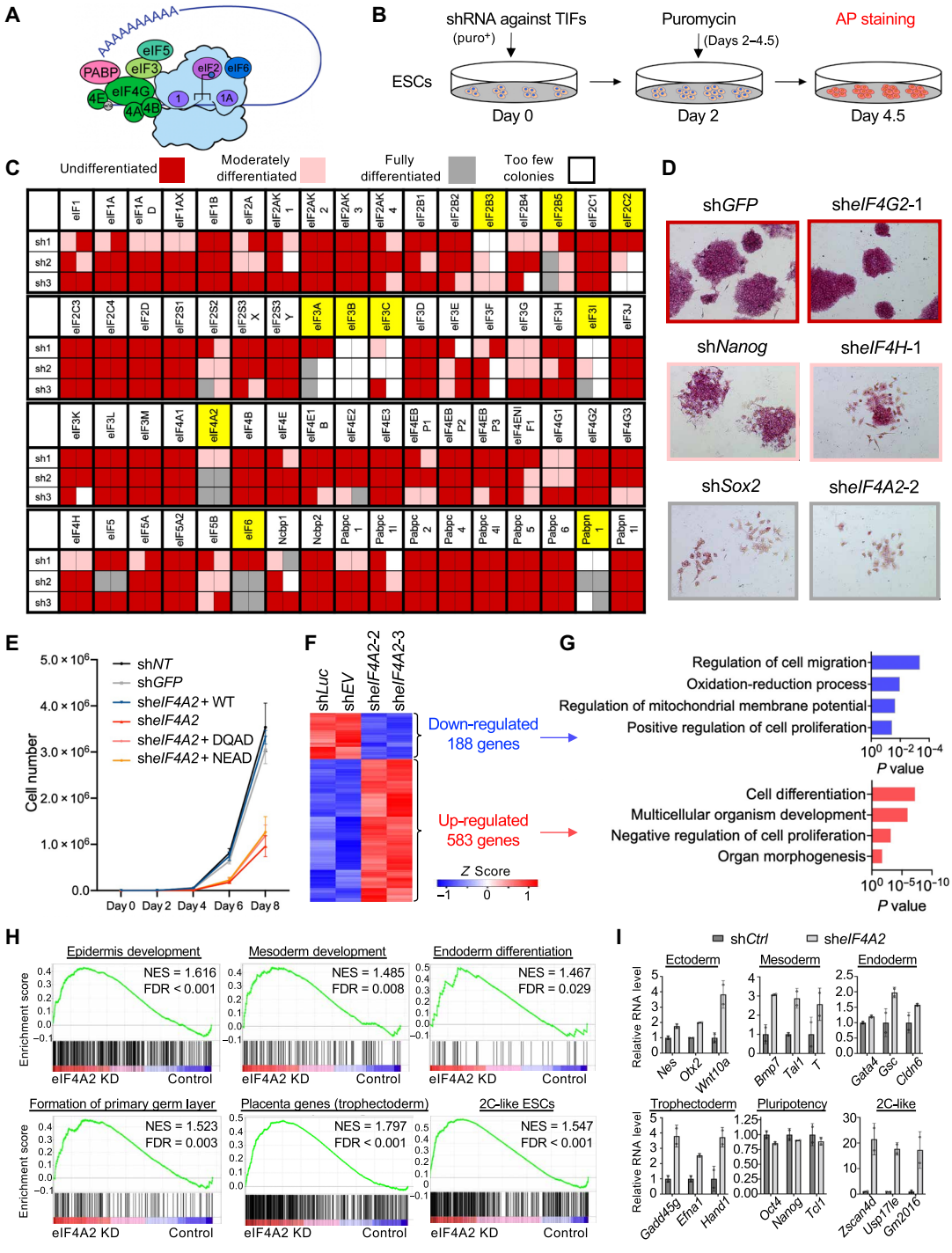

Fig. 1. An RNAi screen identifies the requirement of eIF4A2 for maintaining the ESC identity. (**A**) Schematic of the eukaryotic cap–dependent translation initiation process. PABP, polyadenylate-binding protein; Ncbp1, nuclear cap binding protein subunit 1. (**B**) Schematic of the RNAi screen to identify TIF dependency in ESCs. Puro$^+$ indicates that the shRNA plasmid contains a puromycin-resistant gene. AP is alkaline phosphatase. (**C**) The RNAi screen results. The box colors denote ESC states as indicated. The selected candidates are highlighted in yellow. sh1 to sh3 are three short hairpins for each gene, and screening was performed in biological replicates. (**D**) Representative examples of the AP-stained colony results from the RNAi screen, including the positive controls (sh*Nanog* and sh*Sox2*) and the negative control (sh*GFP*). The border colors match the box colors used in (C). (**E**) Proliferation curves for ESCs with control KD (sh*NT* and sh*GFP*), eIF4A2 KD (she*IF4A2*), eIF4A2 KD rescued with WT eIF4A2 (she*IF4A2* + WT), or helicase activity mutants of eIF4A2 (she*IF4A2* + DQAD/NEAD). (**F** and **G**) Heatmap (F) and Gene Ontology (GO) analysis (G) of the up-regulated and down-regulated transcripts upon eIF4A2 KD from RNA-seq data. shLuc, shLuciferase; EV, empty vector control. (**H**) GSEA results of primary germ layer gene sets (epidermis development, mesoderm development, endoderm differentiation, and formation of primary germ layer), placenta (trophectoderm) gene set, and 2C-like ESCs gene set (Z4 event, Zscan4 expression) by comparing eIF4A2 KD with control KD cells from RNA-seq data. NES, normalized enrichment score. (**I**) Examples of the RNA-seq result in multiple groups. sh*Ctrl* (control shRNA) includes sh*Luc* and sh*EV* control KD experiments.

we removed eight fitness genes essential to many immortalized and cancer cell types (fig. S1B) (*13*) and one gene likely required for ESC viability (eIF2C2; Fig. 1C). eIF4A2 is the only and most consistent TIF whose depletion causes moderate to severe ESC differentiation instead of cell death (Fig. 1, C and D, and fig. S1C), which is consistent with its specific expression enrichment in preimplantation inner cell mass (ICM) of the blastocyst in vivo (fig. S1D) and its down-regulated expression during retinoic acid or fibroblast growth factor 2 (Fgf2)/Activin A differentiation in vitro (fig. S1, E and F).

Next, we validated the KD efficiency (fig. S1, G, H, and K) and the differentiation phenotype in an alternative ESC line (fig. S1I) and under an alternative pluripotent state of 2i/leukemia inhibitory factor (LIF) (*14*) cultured naïve ESCs (fig. S1, J and K). eIF4A2 KD had a minimal effect on cell death/apoptosis of nonpluripotent NIH 3T3 cells and mouse embryonic fibroblasts (MEFs) (fig. S1, L to N), as well as pluripotent cells (fig. S1O). While eIF4A2 depletion did not affect proliferation of nonpluripotent cells, eIF4A2 KD decreased proliferation of pluripotent ESCs (Fig. 1E). In addition, only wild-type (WT), but not helicase activity dead mutants (DQAD and NEAD) of eIF4A2 (*15*), can rescue the eIF4A2 KD effects on ESC proliferation, morphology, and the expression of differentiation and 2C transcripts (Fig. 1E, and fig. S1, P and Q). These results established the essential role of eIF4A2 in maintaining the pluripotency. However, overexpression of eIF4A2 in ESCs (fig. S2A) had minimal effects on the ESC morphology, proliferation, or expression levels of pluripotency factors (fig. S2, A to D), suggesting that eIF4A2 is not limiting in ESC maintenance. To explore its potential roles in establishing the pluripotency, we study the loss/gain of eIF4A2 in reprogramming of somatic cells to induced pluripotent stem cells (iPSCs). Despite its dispensability in MEFs (fig. S1, M and N), eIF4A2 KD markedly decreased MEF reprogramming efficiency by Yamanaka factors (fig. S2, E to G) (*16*) and also decreased reprogramming efficiency of pre-iPSCs to iPSCs (fig. S2, H to J). However, eIF4A2 overexpression had minimal effects on MEF or pre-iPSC reprogramming efficiencies (fig. S2, E to J). These results together establish the critical roles of eIF4A2 in the maintenance and establishment of stem cell pluripotency.

To characterize the molecular features of eIF4A2-depleted ESCs, we performed RNA sequencing (RNA-seq) of ESCs treated with control shRNAs (sh*Ctrl*) against empty vector (sh*EV*) or luciferase (sh*Luc*) and shRNAs against eIF4A2 (sh*eIF4A2*) (using the same KD and drug selection time points as those for the TIF screen in Fig. 1B and table S1). Gene Ontology (GO) analysis of RNA-seq data of 188 down-regulated genes and 583 up-regulated genes (Fig. 1F) revealed the enrichment of GO terms "positive regulation of cell proliferation" and "negative regulation of cell proliferation," respectively (Fig. 1G), consistent with the compromised growth of eIF4A2 KD ESCs (Fig. 1E). Notably, this proliferation defect of KD ESCs is also associated with increased "cell differentiation," a GO term in the up-regulated gene list (Fig. 1, F and G) without changes in cell death or apoptosis (fig. S1O), suggesting that differentiation is likely the cause for reduced growth of eIF4A2 KD ESCs. Gene Set Enrichment Analysis (GSEA) revealed the enrichment of gene sets representing all primary germ layers and, unexpectedly, placenta (trophectoderm) transcripts as well as zinc finger and SCAN domain containing 4 (Zscan4) event–associated 2C-like ESC transcripts (*17*) in eIF4A2 KD ESCs (Fig. 1H). Despite the up-regulation of the RNA levels of three primary germ layers, trophectoderm, and 2C genes, eIF4A2 KD did not change the RNA levels of master pluripotency genes (Fig. 1I). These results highlight the profound role of eIF4A2 in restricting early developmental potency and embryonic/extraembryonic differentiation potential for ESC maintenance.

eIF4A2 is responsible for translation activation and repression of mRNAs encoding cellular potency factors

eIF4A2 is a TIF, but its depletion did not alter global translation rates in ESCs (Fig. 2A). The lack of a global effect on translation upon eIF4A2 loss was also reported in nonpluripotent NIH 3T3, HeLa, and human embryonic kidney 293 cell lines (*18*, *19*). These results suggest that eIF4A2 likely acts on a specific set of mRNAs for the translation initiation control of stem cell pluripotency.

To identify specific mRNAs whose translation initiation is regulated by eIF4A2 in ESCs, we first identified direct RNA binding targets of eIF4A2 by performing enhanced ultraviolet (UV) cross-linking immunoprecipitation (IP) coupled with high-throughput sequencing (eCLIP-seq) (Fig. 2B) (*20*) with biological replicates, which yielded reproducible results (fig. S3A). The binding peaks of eIF4A2 are enriched in mRNAs, particularly at 5′ untranslated region (5′UTR) and the immediate neighboring region of coding sequence (CDS), an mRNA translation initiation region (TIR) that is crucial for the regulation of translation initiation (Fig. 2C; fig. S3, B and C; and table S2) (*21*). The GO analysis of the enriched binding sites revealed that its targets are important for embryonic development, stem cell maintenance, and regulation of translation (Fig. 2D).

Second, we explored the proteome changes upon eIF4A2 KD using SILAC (stable isotope labeling by amino acids in cell culture)–based quantitative mass spectrometry (MS) (Fig. 2E). Upon eIF4A2 KD, the down-regulated proteins were enriched for amino acid biosynthetic process and stem cell maintenance, whereas the up-regulated proteins were clustered into protein phosphorylation and development-related processes (fig. S3D and table S2). We filtered these proteins with maintained mRNA abundance upon eIF4A2 depletion and only chose the eIF4A2-binding targets, obtaining a list of 267 and 364 proteins that are decreased and increased, respectively, in eIF4A2 KD relative to control KD ESCs (Fig. 2F, fig. S3E, and table S2). These targets were considered as directly subject to the translation initiation control by eIF4A2. Notably, the GO analysis of the down-regulated proteins showed the enrichment of stem cell maintenance as the top term (Fig. 2F), among which are 16 pluripotency-associated factors, including the core transcription factors Nanog, Oct4, and Sox2, and all of them were targeted by eIF4A2 at their TIRs (fig. S3E and table S2). In contrast, the top up-regulated proteins upon eIF4A2 KD were Zscan4c/d (Fig. 2F). This well-known 2C factor can activate its own transcription and the associated 2C molecular program (*17*, *22*), consistent with our GSEA result (Fig. 1H).

Third, we performed ribosome profiling (Fig. 2G) to validate the translational outcome of the above-identified eIF4A2 targets. The ribosome profiling results showed that eIF4A2 KD did not change the ribosome bindings on the housekeeping gene *Vcl* mRNA (encoding Vinculin) or the key global translation control gene *Mtor* mRNA (fig. S3F), confirming that eIF4A2 KD did not change the global translation (Fig. 2A). We then confirmed that a number of pluripotency regulators, including the core factors Nanog, Oct4, and Sox2, are translationally activated by eIF4A2 with maintained mRNA levels but decreased binding of translating ribosomes [ribosome-protected mRNA fragments (RPFs)] upon eIF4A2 KD (Fig. 2H and fig. S3G). The binding of eIF4A2 at TIRs (shaded in green in Fig. 2H and fig. S3G) and decreased protein levels of these pluripotency factors after

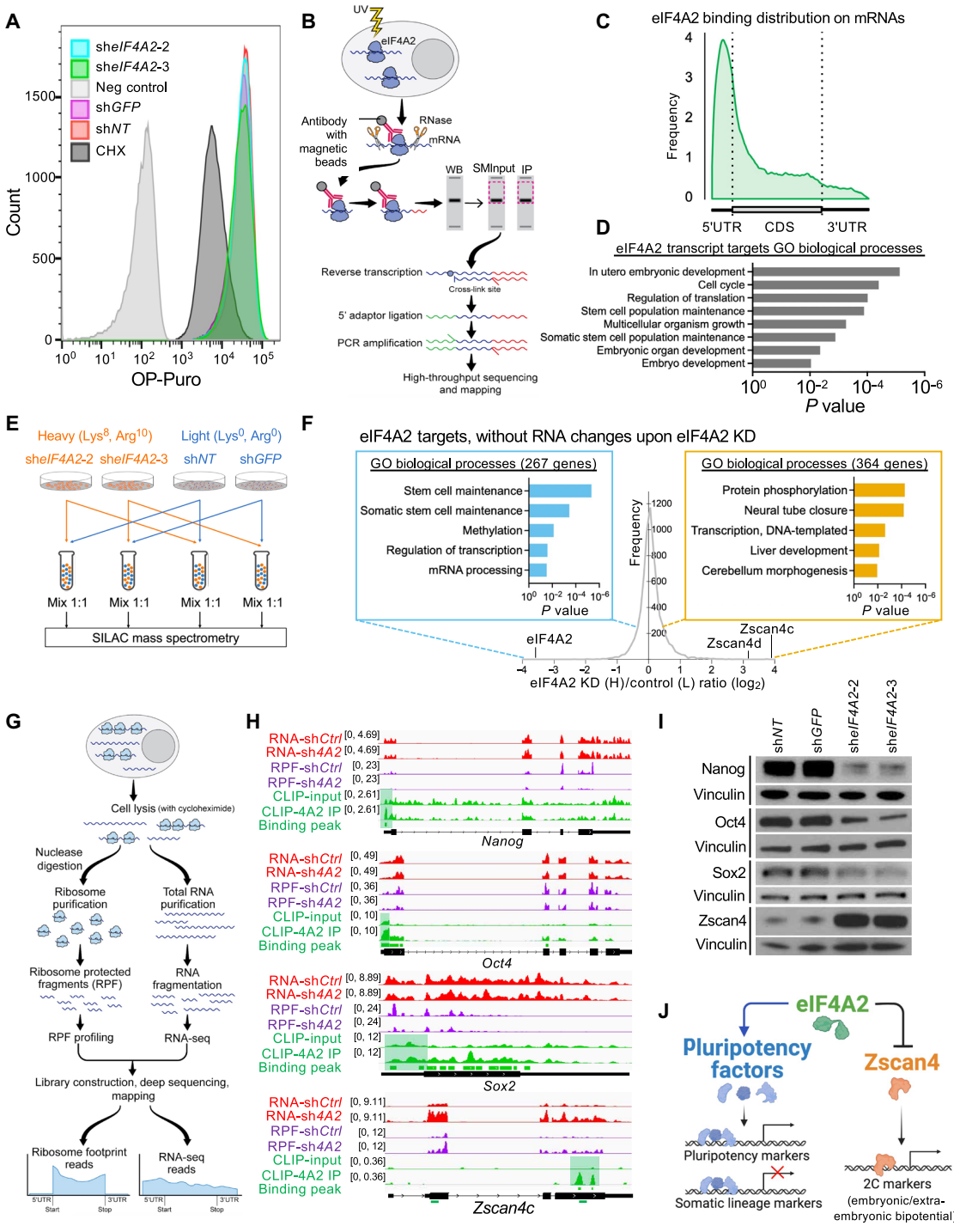

Fig. 2. eIF4A2 acts as both a translation activator and repressor of specific mRNAs encoding cellular potency factors. (**A**) Flow cytometry for OP-puro (*O*-propargyl-puromycin) incorporation in ESCs with control KD and eIF4A2 KD. CHX, cycloheximide, a protein synthesis inhibitor. (**B**) Schematic diagram of the eCLIP-seq protocol. WB, western blot. (**C**) Peak distribution around mRNAs of eIF4A2 targets, identified by eCLIP-seq. (**D**) GO analysis of eIF4A2 targets identified by eCLIP-seq. (**E**) Schematic diagram of SILAC-MS experiment protocol. (**F**) Graph of the frequency distribution of heavy/light (H/L; eIF4A2 KD/control) ratios of all proteins identified by SILAC-MS, with GO analysis of the genes that are targeted by eIF4A2 with decreased (left side, blue box) or increased (right side, orange box) protein levels while maintaining mRNA levels upon eIF4A2 KD. (**G**) Schematic diagram of the ribosome profiling protocol. (**H**) IGV (Integrative Genomics Viewer) snapshots on candidate genes showing RNA-seq (red) and RPF profiling (purple) datasets between control (sh*Ctrl*) and eIF4A2 (sh4A2) KD, and eIF4A2 binding (eCLIP-seq) profiling data (green) with binding of eIF4A2 at TIRs (for *Nanog*, *Oct4*, and *Sox2*) and the CDS of *Zscan4c* near 3′UTR shaded in green. The green marks below the *Zscan4c* gene architecture diagram are the CLIP–quantitative polymerase chain reaction (qPCR) amplicon positions in Fig. 6F. (**I**) Western blots of Nanog, Oct4, Sox2, and Zscan4 in ESCs with control KD and eIF4A2 KD. Vinculin serves as the loading control. (**J**) A model depicting eIF4A2-mediated translation activation of pluripotency transcripts and repression of Zscan4 in ESCs.

eIF4A2 KD (Fig. 2I) were further confirmed. We also confirmed that eIF4A2 KD increased the RNA and RPF levels of Zscan4c/d, the Zscan4 protein levels, and Zscan4$^+$ cells in ESC culture (Fig. 2, H and I, and fig. S3, G and H). Notably, eIF4A2 binds to *Zscan4c/d* mRNAs at the CDS near 3′UTRs instead of TIRs (Fig. 2H and fig. S3G). These results demonstrate that eIF4A2 activates translation initiation of pluripotency transcripts and represses the expression of the totipotency 2C marker Zscan4, which, in turn, restricts embryonic and extraembryonic lineage propensities in ESCs (Figs. 1H and 2J) (*23*).

eIF4A2 depletion affects ribosome binding at TIRs

To explore the mechanism underlying eIF4A2-mediated translation control, we compared genome-wide transcriptional and translational differences upon eIF4A2 depletion. Consistent with observations before, the homodirectional up-regulated genes are enriched with differentiation genes [including trophectoderm markers glial cells missing 1 [Gcm1 (glial cells missing homolog 1)] and Fgf receptor 2 (Fgfr2)] and 2C markers (e.g., Zscan4c/d), and the homodirectional down-regulated genes are enriched for genes involved in negative regulation of mitochondrial fusion, which is also associated with cell differentiation (Fig. 3A, top, and B; fig. S4, A and B; and table S3) (*24*). Notably, upon eIF4A2 depletion, the distribution of ribosome binding is shifted, and the enrichment at TIR observed in the control is lost (Fig. 3C), indicating that eIF4A2 KD compromised the ribosome binding at TIR with a greater extent than the ribosome binding on the other regions of mRNAs. The comparison of transcriptome and translation initiation "regulome" showed that more expression changes upon eIF4A2 KD occurred on the ribosome-binding density at TIR (TIR_RPF, *y* axis), instead of RNA levels (*x* axis) (Fig. 3A, middle, and table S3), and there are more changes happening on TIR_RPF (Fig. 3A, middle) than RPF (Fig. 3A, top).

To identify the candidates through which eIF4A2 exerts the translation initiation control, we applied the stringent criteria to filter the eIF4A2 targets (see details in Materials and Methods). To focus on the molecular mechanisms underlying the ribosome recruitment mediated by eIF4A2, we only focus on the top candidates with the most significant ribosome-binding changes at TIRs upon eIF4A2 depletion. These consist of 60 and 75 genes with translation initiation increase and decrease, respectively, upon eIF4A2 KD (Fig. 3A, bottom, and table S4). Among the 60 up-regulated genes, many genes can induce ESC differentiation or are important for cellular development, such as hexamethylene bis-acetamide inducible 1 (Hexim1) (*25*), transcription factor 12 (Tcf12) (*26*), transcription factor 3 (Tcf3) (*27*), and tet methylcytosine dioxygenase 1 (Tet1) (*28*). Thus, in eIF4A2-depleted ESCs, the overexpression of these genes (at protein level) may contribute to the loss of pluripotency and cellular differentiation. Conversely, among the 75 down-regulated genes, eIF4A2 KD eliminated the ribosome binding at TIRs, observed in the control KD, of many pluripotency regulators (Fig. 2H and fig. S3G). The pluripotency program was thus directly down-regulated through the loss of the translation initiation activation upon eIF4A2 depletion. These results indicate the importance of the translation initiation activation exerted by eIF4A2 in maintaining ESC identity. We, therefore, focused on characterizing the 75 genes whose translation initiation was activated by eIF4A2 to explore how eIF4A2 exerts translation initiation activation control.

eIF4A2 activates target mRNAs via Kozak context–dependent and independent translation initiation

We first examined the ribosome density changes at both TIR and full-length (FL) mRNA bodies of those 75 genes, revealing two distinct patterns of RPF's decrease upon eIF4A2 KD (Fig. 3, D to F): (i) the RPF reduction mainly at TIRs without alteration on the rest of mRNA bodies (temporarily defined as "red targets" red lines in Fig. 3D; ribosomal protein S26 (Rps26) as one example in Fig. 3E); (ii) the RPF reduction along FL mRNA bodies encompassing both TIRs and the rest of mRNA bodies (temporarily defined as "blue targets" blue lines in Fig. 3D; Mettl5 as one example in Fig. 3F).

Translation regulation can be driven by functional RNA regulons within TIRs, such as RNA elements and structures (*21*). To understand how eIF4A2 may distinguish the red from blue targets in translation initiation activation, we scanned eIF4A2-binding motifs at TIRs of these targets (Fig. 3G). We found that the Kozak sequence, which functions as the translation initiation site mediating ribosome assembly (*21*), was enriched only in the red group (rank 1 in red; Fig. 3G). Analysis of the sequence enrichment around the start codons revealed that the Kozak consensus is more robust in the red group than in the blue group, considering the consensus with the most critical two nucleotide positions (G at +4, A/G at −3 relative to +1 as the beginning of the start codon) for the Kozak sequence (Fig. 3H). We also noticed a motif with a pyrimidine (C/U) stretch in the eIF4A2-binding motifs at red TIRs (rank 4 in the red; Fig. 3G), a prominent feature of the 5′ terminal oligopyrimidine motif (5′TOP) (*29*). The 5′TOP mRNAs encode various components of mRNA translation machinery, including ribosomal proteins, translation initiation/elongation factors, and some other proteins (*29*). We found six known 5′TOP mRNAs (*eIF3K*, *Hint1*, *Mrps21*, *Plp2*, *Rps26*, and *Rpl15*) in the red group and none in the blue group (Fig. 3I). While examining the transcriptional start sites (TSSs) of the rest of mRNAs using the database of TSS (*30*) and the RefSeq, UCSC resources (fig. S4C), we found 26 red but only 2 blue mRNAs having TOP-like motifs (Fig. 3I) (*31*). Furthermore, compared with the red targets, the blue targets have longer 5′UTR and more complicated RNA secondary structures, resulting in greater minimum free energy estimates (Fig. 3, J and K, and fig. S4, D to F) (*21*).

Notably, pluripotency-associated mRNA targets discussed before are considered as blue targets on the basis of their RPF change patterns (Fig. 2H and fig. S3G) and the following 5′UTR characteristics: Similar to blue targets, pluripotency mRNAs bear weak Kozak consensus sequence (Fig. 3H), no known 5′TOP mRNAs or TOP-like motifs (Fig. 3I), longer 5′UTR (Fig. 3J), greater free energy estimates of 5′UTR (Fig. 3K), and more complicated 5′UTR structures (fig. S4, D to F).

Together, these results indicate that eIF4A2 activates translation initiation of two distinct groups of target mRNAs (red versus blue) depending on their 5′UTR length/sequences/structures and the Kozak consensus at TIRs. RNA regulons can confer ribosome specificity to gene regulation (*21*, *32*). The mRNAs with stringent Kozak sequences and short 5′UTR are known to be encoded by Rps26-containing ribosomes, whereas Rps26-deficient ribosomes enhance translation of mRNAs with weak Kozak sequences and long 5′UTR, clustering in specific regulatory pathways (*33*). We thus hypothesized that Rps26's presence and absence in ribosomes might be responsible for differential translation initiation of eIF4A2-regulated red and blue targets, respectively.

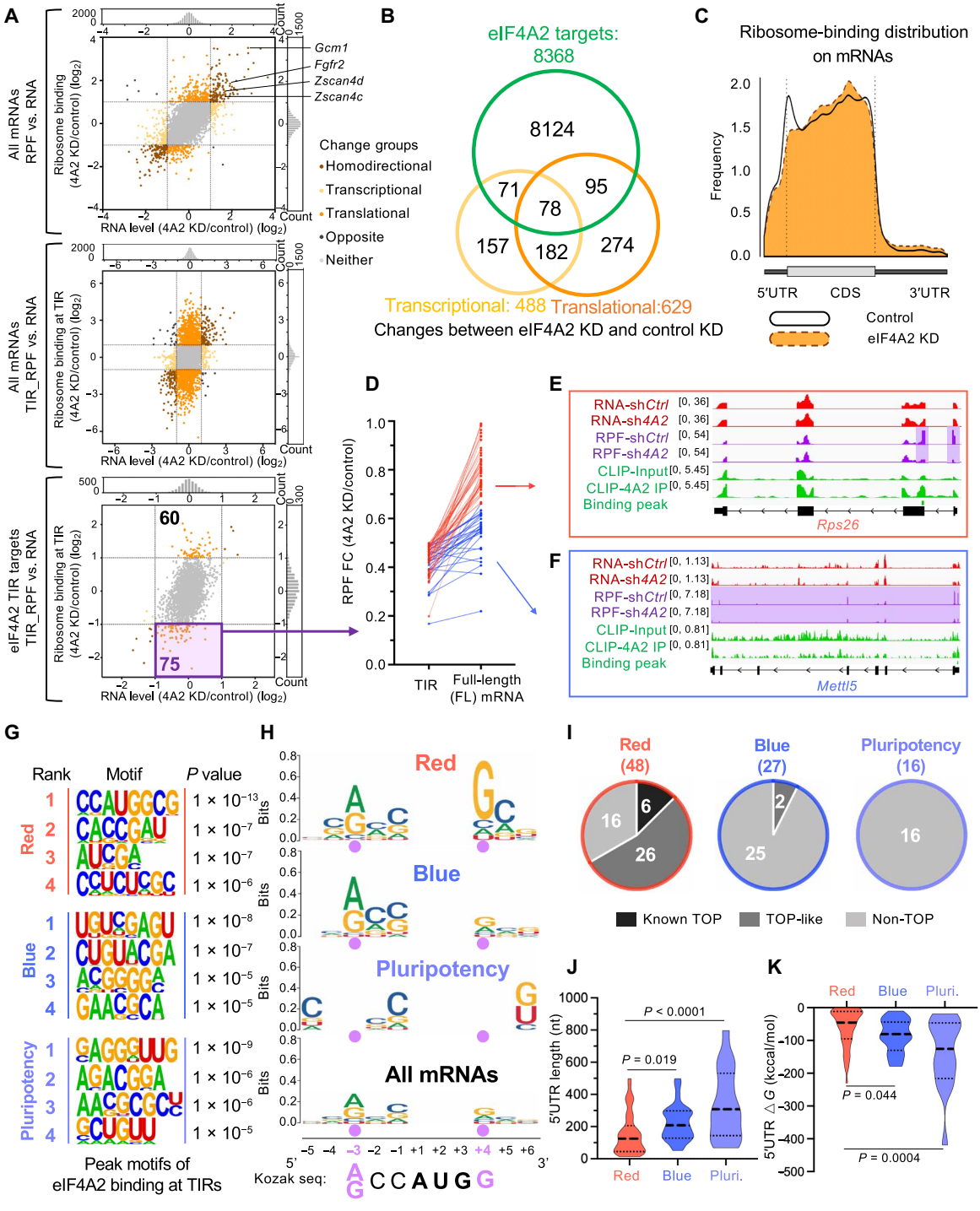

Fig. 3. eIF4A2 activates target mRNAs in two modes of action depending on their 5′UTR complexity and the Kozak consensus at TIRs. (**A**) Transcriptional versus translational (RPF; top) or translation initiation (TIR_RPF; middle) changes of all mRNAs and versus translation initiation changes of eIF4A2 TIR targets (bottom) in eIF4A2 KD relative to control KD ESCs. Targets (75) with ribosome binding at TIR decreased upon eIF4A2 KD are indicated. (**B**) Venn diagram overlapping transcriptional and translational changes upon eIF4A2 KD with eIF4A2 binding targets. (**C**) Ribosome-binding distribution around mRNAs in control and eIF4A2 KD cells, identified by ribosome profiling. (**D** to **F**) eIF4A2 activates the translation initiation of two distinct groups among the 75 direct targets indicated in (A) based on RPF fold change (FC) between eIF4A2 KD and control KD at TIR and full-length (FL) mRNA body, respectively. One representative target of each group is shown in IGV plots (E and F). (**G**) Enriched motifs in eIF4A2 bound peaks at TIRs of the red (top), blue (middle), and pluripotency (bottom) targets. (**H**) Sequence conservation analysis of red, blue, and pluripotency targets around the start codons relative to the Kozak sequence. The two critical consensus nucleotides (−3 and +4) within the Kozak sequence are highlighted with purple dots. (**I**) Pie charts showing the red, blue, and pluripotency targets with known 5′TOP, TOP-like, or non-TOP mRNAs. (**J** and **K**) Graphs showing 5′UTR length (J) and free unfolding energy (in kilocalories per mole) (K) of the red, blue, and pluripotency (pluri.) targets. nt, nucleotide.

Rps26-dependent and -independent translation control can distinguish two modes of translation activation exerted by eIF4A2

To validate the identified features (stringent Kozak sequence and 5′TOP motif) in conferring Rps26-dependent and -independent eIF4A2 functions, we first tested our hypothesis that the pluripotency target mRNAs are preferred by Rps26-deficient ribosomes. Supporting this, ESCs with Rps26 depletion through shRNA-mediated KD maintained both the typical dome-shaped ESC morphology (Fig. 4, A and B) and protein expression levels of the pluripotency targets, such as Klf5, Oct4, and Sox2, and even a slight increase in Nanog protein level (Fig. 4C). In contrast, Rps26 depletion caused the reduced protein abundances (Fig. 4C), but not RNA levels (Fig. 4D), of red targets H3.3 and Suz12, confirming the Rps26-dependent translation of red targets.

We then used the luciferase reporter assays to confirm that 5′UTRs of red and blue targets are functionally effective in mediating translation initiation activation of corresponding luciferase reporter activities, demonstrated by down-regulated luciferase activities upon eIF4A2 depletion, which can be rescued by sh*eIF4A2*-immune *eIF4A2* cDNA (Fig. 4, E to G). We further confirmed Rps26-dependent and -independent functions of eIF4A2 in differential translation control of red and blue targets by showing that the 5′UTR of the red targets, but not the blue targets, down-regulated luciferase activities upon Rps26 depletion, which can be rescued by sh*Rps26*-immune *Rps26* cDNA (Fig. 4, E, G, and H). Notably, the sh*Rps26* targets the CDS of *Rps26* mRNA instead of 5′UTR, so the sh*Rps26* does not target the *Rps26* 5′UTR-luciferase reporter.

Last, we asked whether a minimal alteration (swap) of 5′UTR sequences between red and blue targets would correspondingly alter their translational response to the presence/absence of Rps26. By mutating the red target *Rpl15* 5′UTR with the deletion of its 5′TOP motif and disruption of the Kozak (fig. S5A), we found that the initially responsive and translationally rescuable *Rpl15* 5′UTR became nonresponsive to Rps26 KD or the transgenic rescue with sh*Rps26*-immune *Rps26* cDNA (Fig. 4I). Conversely, by mutating the blue target *Oct4* 5′UTR with the adoption of 5′TOP from the red target *Rpl15* 5′UTR and a single nucleotide change that created an optimized Kozak motif (fig. S5B), we found that the initially nonresponsive *Oct4* 5′UTR became responsive, i.e., down-regulated, to Rps26 KD, which can be translationally rescued by sh*Rps26*-immune *Rps26* cDNA (Fig. 4J). We also confirmed that these mutations did not affect the RNA stability (fig. S5, C and D).

Together, these results showed that eIF4A2 activates translation initiation of its targets in two modes of action, through Rps26-dependent and -independent ribosomes, by recognizing the characteristic features of 5′UTRs, including Kozak sequence and 5′TOP motif. Hereafter, we will mention these red and blue targets as Rps26-dependent and Rps26-independent targets, respectively.

eIF4A2 activates the translation of H3.3 to repress trophectoderm development

We next examined the functional relevance of eIF4A2-mediated translation initiation of the Rps26-dependent targets in maintaining the ESC identity. GO analysis of these targets (table S4) revealed the predominant presence of H3.3-coding *H3f3a* and *H3f3b* genes in 8 of 10 top terms (fig. S6A). Furthermore, supporting Rps26-dependent translation initiation activation of H3.3 by eIF4A2, depletion of Rps26 (Fig. 4, C and D) and eIF4A2 (Fig. 5, A and B, and fig. S6B) led to down-regulation of H3.3 TIR_RPF/protein but not mRNA levels, and the overexpression of Rps26 in eIF4A2 KD cells could rescue the H3.3 protein level partially (Fig. 5, C and D). This eIF4A2-mediated translation initiation activation is highly specific to H3.3, but not H3.1/H3.2, as eIF4A2 KD affects neither ribosome binding on H3.1/H3.2 mRNAs nor H3.1/H3.2 protein synthesis, although eIF4A2 binds to H3.1/H3.2 mRNAs (Fig. 5B, and fig. S6, C and D).

To understand how eIF4A2 binding to H3.3 mRNAs leads to translation activation, we used multiple RNA secondary structure prediction tools (see details in Materials and Methods), which yielded similar predicted structures for *H3f3a/b* 5′UTRs, revealing that most of the eIF4A2-binding sites map to structured stem loops (Fig. 5E and figs. S6E and S7, A and B). Next, we performed the luciferase reporter assays with either mutations or deletions (Δ) of the eIF4A2-binding regions or ribosome-binding regions in *H3f3a/b* 5′ UTRs (Fig. 5, E and F; and figs. S6, E and F, and S7). Our results (Fig. 5F and fig. S6F) revealed: First, all mutants caused various reductions in luciferase activity relative to WT [compare 4 (the bar number, same below), 7, 10, and 13 with 1], indicating that both eIF4A2- and ribosome-binding sites are critical for efficient translation; second, upon eIF4A2 KD, a much larger reduction of luciferase activity was observed for WT reporter (compare 1 with 2) than any other individual mutants (compare each black bar with each light gray bar, such as 4 with 5), indicating that eIF4A2 loss only minimally exacerbates the translational defect already present in each individual mutants; third, upon eIF4A2 KD, ectopic expression of shRNA-immune *eIF4A2* cDNA can rescue the translational defects caused by the loss of eIF4A2 expression in the WT reporters (compare 2 with 3) or the reporters with the mutations/deletions of ribosome-binding sites (compare 11 with 12 and 14 with 15), but not of eIF4A2-binding regions (compare 5 with 6 and 8 with 9). These results are consistent with a general requirement of ribosome binding in translation and, more importantly, highlight a specific contribution of eIF4A2 and its 5′UTR binding to the efficient translation of H3.3.

Depletion of H3.3 was reported to derepress trophoblast lineage genes in ESCs (fig. S6G) through disengagement of PRC2/SUZ12 (another Rps26-dependent target; Fig. 4, C and D) and consequent down-regulation of H3K27me3 (*8*), which was also observed in eIF4A2-depleted ESCs (Fig. 1H) with the decreased H3K27me3 level (Fig. 5B). Comparison of up-regulated genes in H3.3 KD (*8*) and eIF4A2 KD revealed a significant number of overlapped genes with enrichment of GO terms, such as "embryonic placenta development" (Fig. 5, G and H), consistent with the GSEA results (Fig. 1H and fig. S6G). Furthermore, down-regulation of *eIF4A2*, *Rps26*, and *H3f3a/b* was observed during the induction of trophoblast stem cells (iTSCs) from Oct4-depleted ESCs (Fig. 5, I and J, and fig. S6, H and I) (*6*). The depletion of eIF4A2 also facilitated the differentiation of ESCs to iTSCs (Fig. 5K) based on the changes of both the morphology (Fig. 5L) and expression of the pluripotency and TSC markers (Fig. 5M). Last, analysis of the in vivo expression data (*34*) also revealed higher expression levels of *eIF4A2*, *H3f3a*, and *H3f3b* in the blastocyst than the placenta (*Rps26* is not available) (fig. S6J), supportive to our in vitro findings. These results indicate that eIF4A2 participates in Rps26-dependent ribosomes to activate the translation initiation of a specific histone variant H3.3 and together with Suz12, restricting trophectoderm differentiation and safeguarding ESC identity (Fig. 5N).

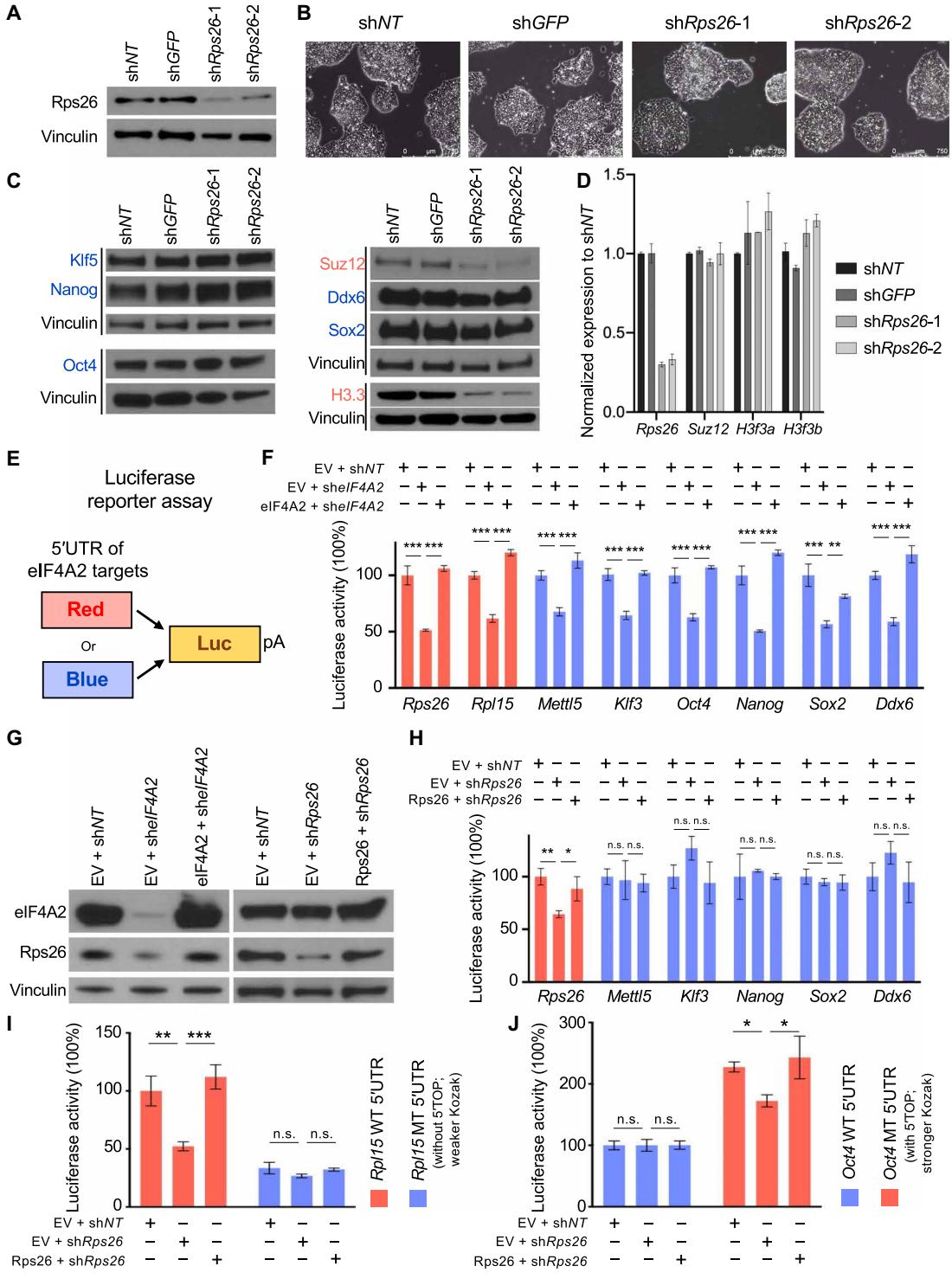

Fig. 4. The two modes of translation activation exerted by eIF4A2 are in Rps26-dependent and -independent control. (**A** and **C**) Western blots of the indicated proteins in ESCs with control KD and Rps26 KD. (**B**) Cell morphology of ESCs with control KD and Rps26 KD. (**D**) The quantitative reverse transcription (qRT)–PCR result of *Rps26*, *Suz12*, *H3f3a*, and *H3f3b* in ESCs with control KD and Rps26 KD, relative to the expression levels in sh*NT* and normalized to β-actin expression. (**E**) Schematic of the luciferase reporter assay. pA, polyadenylation. (**F**) Western blots of the indicated proteins in ESCs expressing the indicated shRNA and plasmid. (**G** and **H**) Luciferase activity in cells transfected with mRNAs containing the 5′UTR of the red or blue target and expressed with the indicated shRNA and plasmid. (**I** and **J**) Luciferase activity in cells transfected with mRNAs containing the WT or mutated 5′UTR of the *Rpl15* (I) or *Oct4* (J) and expressed with the indicated shRNA and plasmid. n.s., not significant. **P* < 0.05, ***P* < 0.01, and ****P* < 0.001.

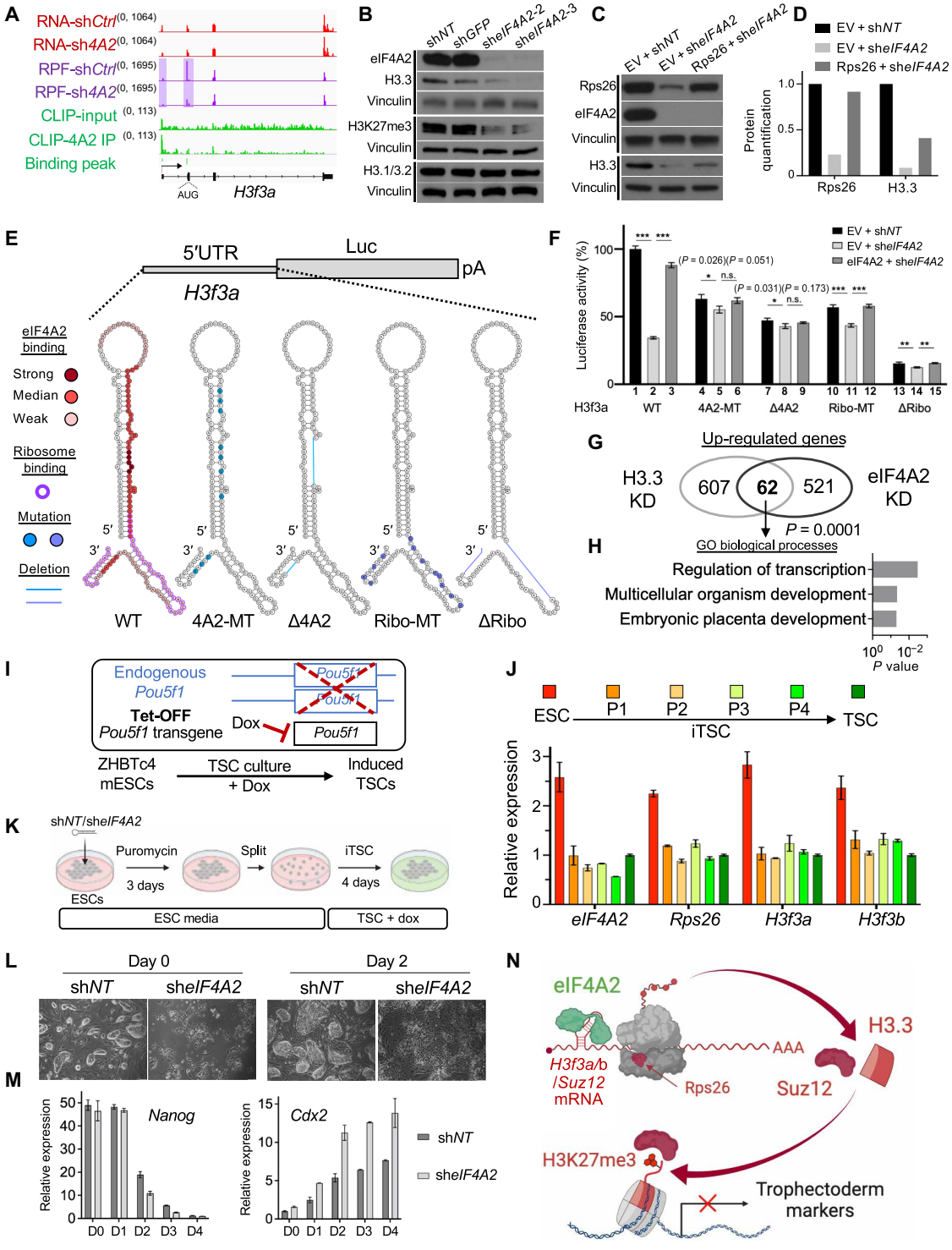

Fig. 5. eIF4A2 activates the translation initiation of H3.3 to inhibit trophectoderm differentiation. (**A**) IGV snapshots on *H3f3a*. The transcription start site and the translation start codon are indicated. (**B** and **C**) Western blots of the indicated proteins between control and eIF4A2 KD ESCs without (B) or with (C) Rps26 rescue. Vinculins serve as loading controls. (**D**) The protein quantification of data in (C), normalized to Vinculin. (**E**) Depiction of luciferase reporter constructs in which the luciferase gene is driven by *H3f3a* 5′UTR WT or mutants (MT) as described in Materials and Methods. (**F**) Luciferase activity of mRNAs driven by the *H3f3a* 5′UTR WT or mutants (MT) in KD and rescue cells. (**G** and **H**) Venn diagrams showing up-regulated transcripts upon eIF4A2 KD or H3.3 KD in ESCs (G) with corresponding GO terms of the overlapped genes (H). (**I** and **J**) Depiction of the TSC induction system (I) and qRT-PCR analysis of indicated transcripts, relative to those in TSCs normalized to β-actin expression, during the ESC-to-TSC transition (J). P1 to P4, passage number, 3 days per passage; TSC, embryo-derived trophoblast stem cells. (**K**) Schematic of TSC induction from ZHBTc4 ESCs with control KD (sh*NT*) or eIF4A2 KD (she*IF4A2*). (**L** and **M**) Morphology (L) and qRT-PCR analysis (M) of sh*NT* or sheIF4A2 KD cells during iTSC induction. (**N**) A model depicting eIF4A2-mediated translation initiation activation of H3.3 in the inhibition of extraembryonic trophectoderm in ESCs. **P* < 0.05, ***P* < 0.01, and ****P* < 0.001.

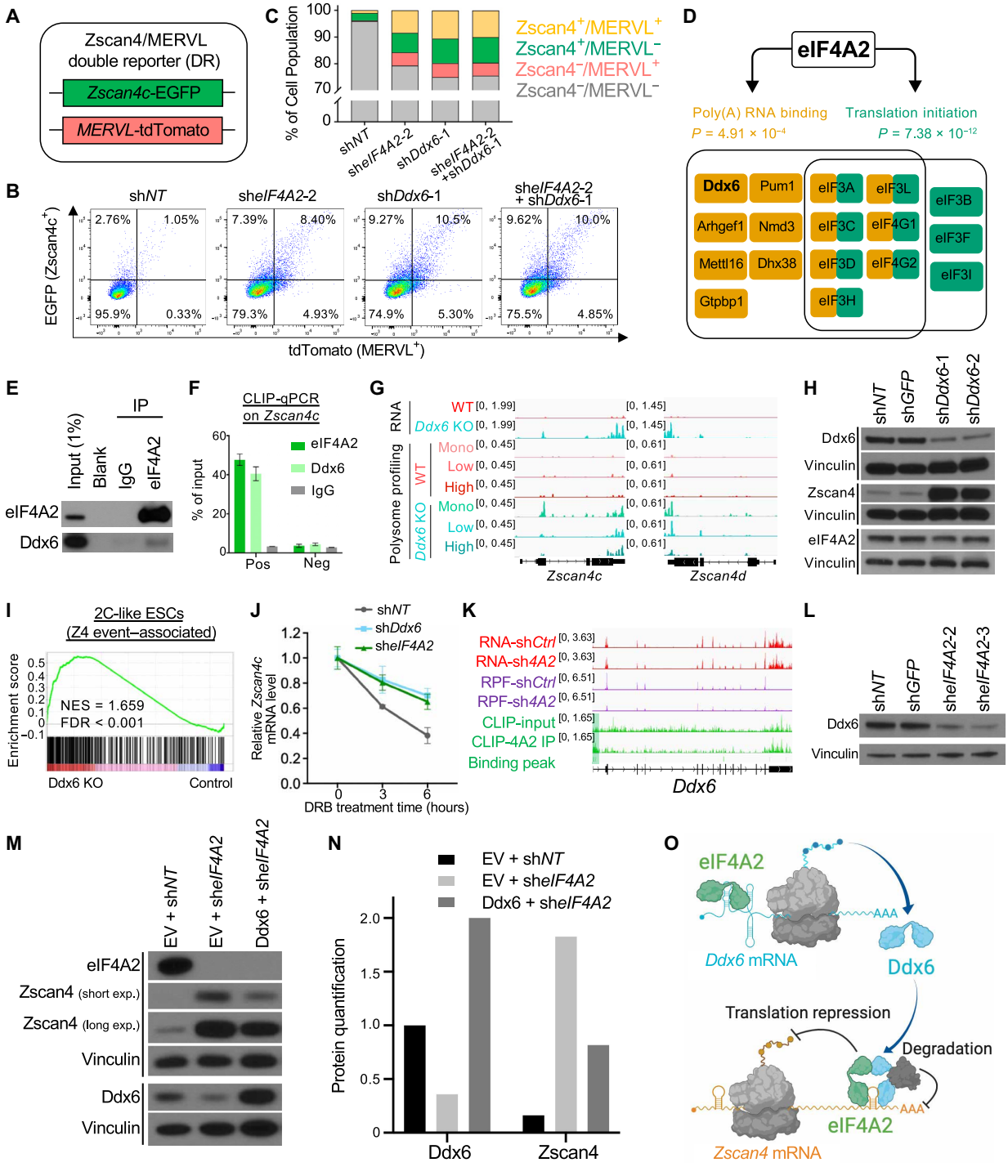

Fig. 6. eIF4A2 represses the 2C gene Zscan4 through the interaction with Ddx6. (**A**) Depiction of the double-reporter system with *Zscan4c*-EGFP and *MERVL*-tdTomato. (**B** and **C**) The flow cytometry (B) and the quantification (C) results of indicated populations in single and double KD cells as shown. (**D**) Depiction of the eIF4A2 interactome with the top two GO terms and associated proteins. Poly(A), polyadenylate. (**E**, **H**, **L**, **M**, and **N**) Western blots of the indicated proteins under treatments as indicated. Vinculin serves as the loading control. The protein quantification in (N) is normalized to the Vinculin protein density in (M). (**F**) CLIP–quantitative PCR on *Zscan4c* with eIF4A2, Ddx6, or immunoglobulin G (IgG) pulldown. The amplicon positions are labeled in Fig. 2H. (**G**) IGV snapshots on *Zscan4c/d* showing RNA-seq data (top two), polysome profiling data for monosome (mono), low polysome (low), and high polysome (high) (middle three and bottom three) between control WT (middle three) and *Ddx6* KO (bottom three). RNA-seq and polysome profiling data are from GSE112765 and GSE112761 (*38*). (**I**) GSEA result of the 2C-like ESCs (Z4 event, Zscan4 expression) gene set by comparing *Ddx6* KO with control cells. (**J**) qRT-PCR of *Zscan4c* in sh*NT*-, sh*Ddx6*-, or she*IF4A2*-infected ESCs with the treatment of the transcription inhibitor DRB (5,6-dichlorobenzimidazole 1-β-D-ribofuranoside, 100 μM) at different time points. (**K**) IGV snapshots on *Ddx6* with similar datasets are shown in Fig. 2H. (**O**) A model depicting eIF4A2-mediated translation initiation activation of Ddx6 and the cooperation between eIF4A2 and Ddx6 in the inhibition of Zscan4 in ESCs.

eIF4A2 activates and interacts with Ddx6 to inhibit the totipotency 2C marker Zscan4 RNA and protein

Apart from roles in translation activation, eIF4A2 is also responsible for translation repression of many differentiation-promoting genes such as Heximl (*25*), Tcf12 (*26*), Tcf3 (*27*), and Tet1 (*28*) (Fig. 3A, bottom). Given that Zscan4 was the most up-regulated protein (Fig. 2F) with a concomitant increase in the double-positive (Zscan4$^+$/MERVL$^+$) 2C-reporter (*35*) populations in eIF4A2 KD ESCs (Fig. 6, A to C) and its prominent roles in regulating totipotent 2C-like cells (*5*, *36*), we decided to address how eIF4A2 represses Zscan4 in ESCs.

Zscan4 is a well-established marker of the 2C totipotency program (*36*). To confirm that the double-positive (Zscan4$^+$/MERVL$^+$) cell subpopulation upon eIF4A2 KD was real 2C-like cells but not an intermediate cell population coexpressing the 2C and differentiation markers, we sorted the double-positive (Zscan4$^+$/MERVL$^+$) and double-negative (Zscan4$^-$/MERVL$^-$) ESC subpopulations upon eIF4A2 KD or control KD (two replicates for each group) and performed the RNA-seq (fig. S8A and table S6). The principal components analysis result showed that the double-positive groups upon eIF4A2 KD were the closest to the double-positive groups upon control KD [shnontargeting (shNT)] (fig. S8B). In addition, the GSEA result revealed that the double-positive groups upon eIF4A2 KD even displayed a stronger 2C-like ESC gene expression signature without a significant bias of differentiation signature compared with the double-positive groups upon control KD (fig. S8C). Furthermore, comparison between the transcriptomes of eIF4A2 KD double-positive cells and control KD double-negative cells (equivalent to the predominant pluripotent cell population in WT ESCs) further highlighted the enrichment of 2C gene signature but not differentiation gene signature (fig. S8D). These results together support the repressive roles of eIF4A2 in the 2C totipotency program and disfavor the possibility of Zscan4$^+$ cell populations upon eIF4A2 KD being an intermediate cell population coexpressing 2C and differentiation genes.

The translational repression roles of eIF4A2 was explored in HeLa cells, in which eIF4A2 interacts with the components of the Ccr4-Not deadenylase complex to inhibit the translation of its targets (*37*). To examine whether a similar repressive mechanism exists in ESCs, we performed eIF4A2 IP, followed by MS in ESCs (table S5 and fig. S8E). While many TIFs were identified in the eIF4A2 interactome, supporting its roles in translation initiation, we did not detect Ccr4-Not components, suggesting a potentially different mechanism of eIF4A2 for translational repression in ESCs. Instead of Ccr4-Not members, DEAD-box helicase 6 (Ddx6) was identified in the eIF4A2 interactome in ESCs (Fig. 6, D and E), which was reported to play roles in mRNA degradation and translational repression in ESCs (*38*, *39*). We confirmed the cobinding of Ddx6 and eIF4A2 on *Zscan4c* mRNA (Figs. 2H and 6F). Both RNA and protein up-regulation of Zscan4c/d were observed from RNA-seq and polysome profiling of Ddx6-depleted ESCs compared with WT ESCs (Fig. 6G) (*38*). Ddx6 KD increased Zscan4 protein level (with a minimal effect on eIF4A2 protein level) (Fig. 6H), the Zscan4$^+$ cell population (fig. S8F), and double-positive populations in *Zscan4c*–enhanced green fluorescent protein (EGFP)/*MERVL*-tdTomato double-reporter ESCs (Fig. 6, A to C). Ddx6 depletion also up-regulated Zscan4 expression [i.e., Z4 event (*17*)]–associated 2C-like signature transcripts (Fig. 6I). These data support the involvement of Ddx6 in eIF4A2-mediated Zscan4 repression.

Zscan4 expression is highly heterogeneous in ESC culture (*36*). To examine expression profiling of eIF4A2, Ddx6, and Zscan4 in ESCs, we first analyzed their RNA expression levels in mouse early embryogenesis, revealing that both eIF4A2 and Ddx6 have relatively low expression levels during the 2C stage (figs. S1D and S8G). In ESC culture, the single-cell RNA-seq (*40*) indicates that, compared with the expression patterns of *Oct4* (relatively homogeneous), *Nanog* (relatively heterogeneous/mosaic-in-colony), and *Zscan4c* (highly heterogeneous/spot-in-colony) (*41*), both *eIF4A2* and *Ddx6* are expressed in a rather heterogeneous pattern similar to *Nanog* (fig. S8H). However, when we ranked the cells based on *Zscan4c* RNA expression level [UMIFM (unique molecular identifiers filtered mapped) counts from 0 to 4], neither *eIF4A2* nor *Ddx6* showed obvious *Zscan4c* correlated or anticorrelated RNA expression pattern (fig. S8I), suggesting the important posttranscriptional (including translational) control of these factors. We then performed immunofluorescence to examine their protein levels, revealing relatively heterogeneous expression patterns of eIF4A2 and Ddx6 and confirming the P-body location of Ddx6 in ESCs as reported (fig. S8J) (*38*, *39*). Zscan4$^+$ cells are not present in the cell population with P-bodies (indicated by Ddx6-expressing dots in fig. S8J, middle). However, we did notice a small number of non–P-body Ddx6-expressing cells coexpress Zscan4 with the expression of Ddx6 in a diffused instead of classical P-body–dotted pattern (Zoom-in bottom panels in fig. S8J). We further confirmed that Ddx6 depletion inhibited the degradation of *Zscan4c* mRNA (Fig. 6J). These results suggest a specific role of Ddx6 in the repression of Zscan4 via a P-body–dependent manner (and possibly also a P-body–independent role of Ddx6 in Zscan4 activation).

To lend further support that eIF4A2 and Ddx6 may act together on gene repression, we compared up-regulated genes in eIF4A2 KD (Fig. 1F) and *Ddx6* knockout (KO) cells (*38*). We observed a significant number of corepressed genes enriched in cell differentiation and "multicellular organism development" (fig. S8, K and L), consistent with the differentiation phenotype of both eIF4A2 KD (Fig. 1 and fig. S1) and Ddx6 KD ESCs (fig. S8, M and N) (*38*). However, unlike eIF4A2 KD (Fig. 2, H and I), Ddx6 KD did not down-regulate the protein levels of Oct4/Nanog/Sox2 (fig. S8, O and P). eIF4A2 binds to the TIR of *Ddx6* mRNA and translationally activates Ddx6, supported by the maintained mRNA abundance but decreased RPF levels of Ddx6 upon eIF4A2 KD (Fig. 6K). On the basis of the RPF change pattern, Ddx6 is an Rps26-independent target under eIF4A2-mediated translation initiation activation, confirmed by the luciferase reporter assays and western blot of Ddx6 in eIF4A2- or Rps26-depleted ESCs (Figs. 4, C, G, and H, and 6L). eIF4A2 KD also prevented degradation of *Zscan4c* mRNA, consistent with Ddx6 depletion (Fig. 6J). Moreover, while double KD of eIF4A2 and Ddx6 did not synergize the up-regulation of the 2C-like population compared with the single depletion (Fig. 6, A to C), overexpression of Ddx6 partially but not fully rescued the up-regulation of Zscan4 protein level in eIF4A2-depleted ESCs (Fig. 6, M and N), suggesting that eIF4A2 and Ddx6 may function through the same pathway to regulate the 2C-like subpopulation in ESCs and that additional factors other than Ddx6 may also contribute to eIF4A2-mediated repression of Zscan4 abundance (see Discussion). Together, these results establish a model whereby eIF4A2 restricts the totipotency 2C program by activating the translation initiation of *Ddx6* mRNA and recruiting Ddx6 protein for Zscan4 mRNA degradation and translational repression in maintaining pluripotency of ESCs (Fig. 6O).

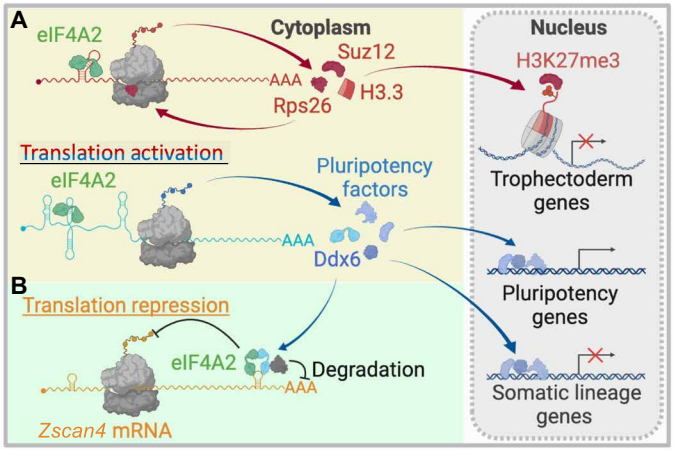

Fig. 7. A model depicting eIF4A2-mediated translational control in safeguarding ESC identity. eIF4A2 is responsible for a unique translation initiation control network dedicated to safeguarding ESC identity. (**A**) eIF4A2 binds to the TIR of its targets to activate the translation initiation: eIF4A2 activates the translation initiation of H3.3 and Rps26 through Rps26-dependent ribosomes (red); eIF4A2 also activates specific pluripotency-associated mRNAs and Ddx6 through Rps26-independent ribosomes (blue). (**B**) Via the physical interaction with Ddx6, eIF4A2 represses Zscan4's expression by binding CDS near 3′UTR (non-TIR) of *Zscan4* mRNAs (orange).

DISCUSSION

We demonstrate that eIF4A2 is specifically responsible for a unique translation initiation control mechanism dedicated to safeguarding ESC identity through restricting embryonic/extraembryonic differentiation and the totipotency 2C program (Fig. 7). On the one hand, eIF4A2 activates the translation initiation of histone variant H3.3 (together with Polycomb protein Suz12) and pluripotency factors possibly through Rps26-dependent and -independent mechanisms, respectively, distinguished by RNA characteristics or regulon (i.e., RNA sequence elements and structural complexity) surrounding the start codon and the 5′UTR, leading to the activation of pluripotency program and repression of multilineage differentiation (Fig. 7A). On the other hand, eIF4A2 translationally activates *Ddx6* mRNA and interacts with Ddx6 in binding CDS near 3′UTR of *Zscan4* mRNAs, leading to Zscan4 mRNA degradation and translation repression in restricting totipotency 2C program in pluripotent cells (Fig. 7B). We thus established a translational paradigm in the cytoplasm for the protein synthesis of stem cell potency transcription factors (e.g., Oct4, Sox2, Nanog and Zscan4) and epigenetic regulators (e.g., H3.3 and Suz12) imposed on their well-established transcriptional roles in the nucleus in promoting pluripotency and repressing trophectoderm/totipotency. Lending further support of our findings, eIF4A2-constitutive KO mice were embryonic lethal (www.taconic.com/knockout-mouse/eif4a2-trapped) (Taconic Biosciences Inc.), and both mouse (fig. S1, J and K) and human (*42*) naïve ESCs rely on eIF4A2-dependent, but not eIF4A1-dependent, pathways to form a more compact naïve proteome for translating selective mRNAs (*42*).

An outstanding question remains as to why ribosome binding is only lost at TIR instead of FL mRNA bodies upon eIF4A2 depletion for the Rps26-dependent targets. Emerging evidence shows that ribosomes can be stalled on transcripts during translation elongation (*43*, *44*). mRNA translation is an energy-consuming process (*45*). 5′TOP transcripts are highly abundant, and they are best-translated by the heavy polysomes, and a small perturbation in these 5′TOP RNA-coding protein levels can lead to an acute and profound impact on broad downstream translation events (*46*, *47*). Thus, ribosome stalling can avoid wasting dedicated energy and provide a rapid response to deter the current ongoing 5′TOP translation products. Upon eIF4A2 KD and Rps26 down-regulation, Rps26-independent ribosomes of high abundance, which may be enriched in monosomes and/or light polysomes under the normal condition, may start to bind and translate the Rps26-dependent targets, causing stalling and trigger *cis*-acting feedback inhibition of translation initiation (*48*). This can help explain the loss of ribosome binding at TIRs but no other regions on the Rps26-dependent targets upon eIF4A2 depletion. Moreover, for the differences around the start codons among the Rps26-dependent/independent targets (Fig. 3H), apart from the differences around the "−4" position, where Rps26 binds (*33*), differences were also observed at −3, −5, and +4 positions, which could be due to the overall ribosome structural changes upon Rps26 depletion altering the whole ribosome-binding profile on mRNAs. Although Rps26 was reported substoichiometric in free ribosome subunits relative to heavy polysomes in mouse ESCs (*49*), it remains to be determined whether it is substoichiometric in monosomes/light polysomes. It is also formally possible that ribosomal proteins other than Rps26 in the eIF4A2 translatome may act alone or together with Rps26 in contributing to the functional specialization of eIF4A2 for translational control of stem cell pluripotency, a topic worthy of more investigations.

The Rps26-dependent targets also include H3.3-coding mRNAs. We did not detect H3.3 in the SILAC-MS assay (table S2), which may be due to the highly similar peptide sequences between H3.3 and H3.1/H3.2, as well as the highly K/R-rich histone peptides that may be overdigested by trypsin in SILAC-MS. Unlike canonical H3.1/H3.2 mRNAs with stem-loop structures at 3′UTRs for stem-loop binding protein (SLBP)–mediated translation (*50*), H3.3 mRNAs are non-canonical with introns, polyadenylated tails, and longer 5′UTRs/3′UTRs without stem-loop structures at 3′UTRs. These unique features potentially endow H3.3 with distinct gene expression control. Our study identified an eIF4A2-mediated translation initiation activation of H3.3 in ESCs with Rps26-dependent ribosomes. The role of H3.3 during early development and the recurrent mutations of H3.3 in multiple types of cancers have been well recognized (*51*), highlighting the importance of our findings on translation control of H3.3 in further understanding its roles in development and disease.

We showed that eIF4A2 activates the translation initiation of pluripotency-associated mRNAs through Rps26-independent ribosomes. Mettl3 and Mettl14, two components of the methyltransferase complex, are the targets underlying this translation initiation control (table S2), which deposit N^6-methyladenosine (m^6A) on key pluripotency transcripts to promote their degradation (*52*). This raises an intriguing possibility: eIF4A2 KD decreases protein synthesis of key pluripotency factors, but their mRNA levels, which are supposed to be down-regulated as well on the basis of the feedforward transcriptional circuitry (*23*), are maintained. This can be explained by the stabilization of these mRNAs with reduced m^6A modifications (*52*), resulting from reduced protein levels of Mettl3/14 whose mRNAs are subject to eIF4A2-mediated translation initiation activation. Future investigation is needed to validate this potential mechanism.

Embryonic development is associated with the stepwise restriction of cell potency from totipotent 2C embryos to pluripotent ICM

of the blastocyst (*53*); accordingly, pluripotency may require a proper restriction of the totipotency 2C program in ESCs. In ESCs, the expression of Zscan4 is transient and reversible in only 1 to 5% of the cell population (*17*), and overexpression of Zscan4c in ESCs activates MT2/MERVL and 2C genes (including *Zscan4* cluster) (*22*), indicating an elaborate mechanism in ESCs responsible for the repression of Zscan4 and the associated 2C program. Here, we presented a previously unidentified mechanism of eIF4A2-mediated repression of Zscan4 in ESCs, partly through Ddx6. The derepression of Zscan4 upon eIF4A2/Ddx6 KD emerged in only a subpopulation of ESCs (figs. S3H and S8F), which may explain the low magnitude in bulk RNA expression changes of 2C markers (table S1). DDX6 can also be recruited to 5′UTRs of some eIF4A2 TIR targets (*39*), which warrants future investigation for their potential collaborative or competitive roles in target gene expression control. H3.3 also impedes the 2C program in ESCs (*54*). It remains to be determined how eIF4A2-mediated translation repression and activation of Zscan4c/d and H3.3, respectively, may cross-talk or synergize in restricting the 2C program in ESCs and early development. Last, apart from Ddx6, eIF4A2 may enlist other factors in the eIF4A2 interactome, such as pumilio RNA-binding family member 1 (Pum1), to restrict 2C and lineage differentiation in maintaining the ESC identity. Pum1 is a posttranscriptional and translational repressor found in P-bodies and stress granules, and it can promote ESC differentiation during exit from pluripotency (*55*). In undifferentiated ESCs, eIF4A2 may sequester Pum1 through their physical association and restrict its functions to prevent ESC differentiation, which warrants future investigation. Moreover, as Ddx6 and Pum1 can also be involved in microRNA (miRNA)–mediated repression (*56*, *57*), we do not exclude the possibility that eIF4A2 may also be involved, indirectly, in the repression of certain mRNAs via miRNA-related functions in ESCs.

MATERIALS AND METHODS

Murine ESC culture

Feeder-free murine ESCs were grown on 0.1% gelatin-coated plates in ESC medium containing high-glucose Dulbecco's modified Eagle's medium (DMEM), 15% fetal bovine serum (FBS), 100 μM nonessential amino acids (NEAA), 1% nucleoside mix, 2 mM L-glutamine, penicillin-streptomycin (50 U/ml), 0.1 mM 2-mercaptoethanol, and homemade recombinant LIF tested for efficient self-renewal maintenance, at 37°C and 5% CO_2. For naïve culture conditions (2i/LIF), murine ESCs were cultured on 0.1% gelatin-coated plates using serum-free N2B27 medium (DMEM/F12 and Neurobasal media were used in a ratio of 1:1, 1× B27 supplement, 1× N2 supplement, penicillin-streptomycin (50 U/ml), 2 mM L-glutamine, and 0.1 mM 2-mercaptoethanol) supplemented with glycogen synthase kinase 3β inhibitor (CHIR99021, 3 μM final), mitogen-activated protein kinase kinase inhibitor (PD0325901, 1 μM final), and recombinant LIF.

Construction of WT and mutant 5′ UTR-driven luciferase plasmids

For luciferase reporter assays, the indicated 5′UTR sequences were synthesized at Integrated DNA Technologies and inserted into the pGL3 luciferase reporter vector using Hind III and Nco I sites. The details for the 5′UTR construction in Fig. 5E and fig. S6E are the following: WT; MT, the mutant with mutations that disrupt the eIF4A2 (4A2-MT) or ribosome (Ribo-MT)–binding region; Δ4A2/ΔRibo, the mutant with the deletion of eIF4A2 (Δ4A2) or ribosome (ΔRibo)–binding site. In WT, red indicates eIF4A2 binding with the gradient denoting the binding strength; purple indicates the ribosome binding. In mutants, blue/violet nucleotides and lines indicate the mutation and the deletion, respectively, in the eIF4A2 (blue)/ribosome (violet)–binding regions.

TSC culture and iTSC reprogramming

ZHBTc4 ESCs (*6*) are cultured in serum + LIF ESC medium. For iTSC, medium was replaced to TSC medium [RPMI 1640 supplemented with 20% FBS, penicillin-streptomycin (50 U/ml), 0.1 mM 2-mercaptoethanol, 2 mM L-glutamine, 100 μM NEAA, recombinant FGF4 (25 ng/ml), and heparin (1 μg/ml)] supplemented with doxycycline (Dox) (1 μg/ml).

Transfection and lentiviral infection

Transfection of cells was performed using Lipofectamine 3000 according to the manufacturer's manual. The production of lentivirus and viral infection were performed as described (*58*). All shRNA KD experiments followed the same time points as the RNAi screen, which ended on day 4.5 with 2.5-day drug selection (puromycin,1 μg/ml).

RNAi screen

To perform a TIF RNAi screen, we selected the constitutive shRNAs (three independent shRNAs per gene) with validated KD efficiencies wherever data were available in the literature. For those that have not been reported, we selected three independent shRNAs with the best-predicted KD efficiency targeting both exons and 3′UTR regions. The lentivirus was prepared as previously described (*58*). ESCs were seeded in the gelatin-coated tissue culture plates together with the viruses for viral infection (details as previously described) (*58*) (day 0). On day 1, the virus/medium was changed with regular serum/LIF ESC medium. From day 2, the medium was changed with serum/LIF ESC medium containing puromycin (1 μg/ml) daily to select the infected cells. The negative control for drug selection showed that the drug treatment killed all uninfected cells after 2 days. On day 4.5, AP staining was performed to record the phenotype.

This screen identified eIF4A2 as the TIF specifically required for ESC maintenance from an RNAi screen of all factors involved in translation initiation. To our knowledge, this is the first screen specifically focused on the translation initiation machinery. Many large-scale RNAi/CRISPR screens collected results 48 or 72 hours after introductions of short RNAs (shRNA/small interfering RNA/single guide RNA) against targets (*59*–*62*), but as median half-lives of eukaryotic mRNAs and proteins are 9 and 46 hours separately (*63*), a lot of important candidates were overlooked because of the presence of their undegraded proteins at the end of those screens. These time points are particularly important for the factors involved in translational control as it would take longer for their targets to have responses in their protein levels. Therefore, we ended our screen at day 4.5 after infection. This time point is indeed important as upon eIF4A2 KD, the loss of the dome-shaped ESC morphology started around 3.5 days later, explaining why eIF4A2 was overlooked by many previous screens. In addition, we recorded screen results with AP staining, a direct phenotypic marker of pluripotent stem cells, instead of transgenic reporters used in many other studies (*59*–*61*). Transgenic reporters are proper and sensitive to transcriptional change while not suitable for identifying direct translational change, and they are limited to the response of certain transcriptional regulatory elements.

iPSC reprogramming

MEF reprogramming was performed as described (*16*) with a few modifications. Briefly, 100,000 reprogrammable MEFs containing a Dox-inducible OKSM (Oct4, Klf4, Sox2, and c-Myc) cassette were infected with shRNA lentiviruses or transfected with plasmids, followed by puromycin (1 μg/ml) or hygromycin (250 μg/ml). After the drug selection, 95,000 MEFs were seeded on top of irradiated MEF feeders on a 12-well tissue culture plate coated with gelatin, in Dox-containing serum/LIF ESC medium (day 0). From day 13, the medium was changed to serum/LIF ESC medium without Dox until day 19, when AP-staining was performed to record the reprogramming result.

MEF-derived Nanog-GFP pre-iPSCs were maintained and used for reprogramming as described (*64*). Briefly, MEF-derived Nanog-GFP pre-iPSCs were infected with shRNA lentiviruses or transfected with plasmids. A total of 20,000 pre-iPSCs were seeded after selection on a 12-well tissue culture plate coated with gelatin and grown in serum + LIF for 2 days before medium switch to 2i + LIF. On day 10 in 2i + LIF, Nanog-GFP iPSC colonies were counted under fluorescence microscopy.

Immunofluorescence staining

Cells were fixed with 4% paraformaldehyde (w/v) for 15 min at room temperature, washed, then permeabilized with 0.25% Triton X-100 solution for 5 min at room temperature, and blocked with 5% FBS. Then, cells were incubated with primary antibodies and 5% FBS in phosphate-buffered saline (PBS) overnight at 4°C. The next day, after washing, cells were incubated with secondary antibodies and 3 μM 4′,6-diamidino-2-phenylindole with 5% FBS in PBS for 1 hour at room temperature in the dark. After washing, cells were imaged with a Leica DMI 6000 inverted microscope.

Whole-cell extract preparation, co-IP, and Western blot

Whole-cell lysates were harvested from ESCs in lysis buffer [50 mM Hepes (pH 7.6), 250 mM NaCl, 0.1% NP-40, 0.2 mM EDTA, 1.4 mM β-mercaptoethanol, 0.2 mM phenylmethylsulfonyl fluoride (PMSF), and 1× protease inhibitor cocktail], and before IP, NaCl concentration of the lysates was diluted to 179 mM with dilution buffer [20 mM tris (pH 7.6), 20% glycerol, 0.05% NP-40, 0.2 mM EDTA, 1.4 mM β-mercaptoethanol, 0.2 mM PMSF, and 1× protease inhibitor cocktail]. The lysates were incubated with the anti-eIF4A2 antibody or immunoglobulin G (IgG) control by rotating overnight at 4°C. On the 2nd day, Protein G agarose beads were equilibrated with lysis buffer diluted with dilution buffer (179 mM NaCl). The lysate/antibody mixtures were added to the equilibrated beads and rotated for 3 hours at 4°C. The bound beads were washed five times with wash buffer [50 mM Hepes (pH 7.6), 179 mM NaCl, 0.1% NP-40, 0.2 mM EDTA, 1.4 mM β-mercaptoethanol, and 0.2 mM PMSF] and then eluted with SDS–dithiothreitol (DTT) loading buffer by boiling for 5 min at 95°C. Eluted proteins were separated by SDS–polyacrylamide gel electrophoresis (PAGE) and visualized by Western blotting. Trueblot secondary antibody was used to reduce the IgG detection.

IP of eIF4A2 protein complexes in ESCs and liquid chromatography–tandem MS analysis

To identify eIF4A2-interacting partners in ESCs, we used three different anti-eIF4A2 antibodies [IP1: ab194471 (mouse polyclonal, Abcam), IP2: ab31218 (rabbit polyclonal, Abcam), and IP3: PA5-27431 (rabbit polyclonal, Thermo Fisher Scientific)] to isolate eIF4A2 protein complexes independently for MS identification, with IgG pulldown as controls (for ab194471, the control was a normal mouse IgG polyclonal antibody, 12-371 from Sigma-Aldrich; for ab31218 and PA5-27431, the control was a normal rabbit IgG polyclonal antibody, PP64 from MilliporeSigma). Whole-cell lysates were prepared as previously described from 20 cm–by–15 cm dishes of WT ESCs. Then, to decrease the salt concentration to 100 mM, the lysates were transferred to a dialyzer with dialysis buffer [20 mM Hepes (pH 7.9), 20% glycerol (v/v), 100 mM KCl, 1.5 mM $MgCl_2$, 0.2 mM EDTA, 0.5 mM DTT, 0.2 mM PMSF, and 1× protease inhibitor cocktail] at 4°C for 3 hours. The precipitated proteins were removed by centrifugation. Then, the total protein mass of the lysates was determined after protein concentration measurement. Ten milligrams of proteins were used for each IP, and some lysates were left as Input. IP lysates were diluted with dialysis buffer supplemented with 0.02% NP-40 (dubbed IP-DNP) to 12 ml, and Benzonase (20 μl, 15 U/μl; Pierce) was added to remove DNA and RNA. The lysates were precleared with 100 μl of IP-DNP buffer–equilibrated Protein G agarose beads per 10 mg of total protein for 1 hour at 4°C, followed by incubation with 20 μg of anti-eIF4A2 antibody (or IgG) by rotating overnight at 4°C. On the 2nd day, Protein G agarose beads were equilibrated with IP-DNP buffer. The lysate/antibody mixtures were added to the equilibrated beads and rotated for 3 hours at 4°C. After the bound beads were washed five times with IP-DNP buffer, the protein complexes were eluted with SDS loading buffer by boiling for 5 min at 95°C and separated by an SDS-PAGE gel. Whole lanes were excised and subjected to liquid chromatography–tandem MS (LC-MS/MS) analysis. MS data were processed by Thermo Proteome Discoverer software with SEQUEST engine against Swiss-Prot mouse protein sequence database. Proteins were filtered by the minimal number of identified unique peptides (≥2). Common contamination proteins (e.g., keratins) were removed, and spectral count (the number of peptide spectrum matches) ratio of (eIF4A2 IP/IgG) ≥4 was applied. The list was cleaned with CRAPome (*65*). The lists for three IP/IgG groups with spectral count ratios are present in table S5. Of the three lists, the proteins presented in at least two lists were combined as the final eIF4A2 interactome in ESCs for GO analysis (Fig. 6D).

SILAC-MS profiling of relative protein levels

ESCs were cultured in the medium labeled by either light (L-arginine and L-lysine) or heavy (L-$^{13}C_6{}^{15}N_4$-arginine and L-$^{13}C_6{}^{15}N_2$-lysine) for more than 2 weeks. The cells cultured in light and heavy media were infected with control shRNAs and eIF4A2 shRNAs, respectively. The infected cells were selected by puromycin (1 μg/ml), and the cell lysates at different SILAC media were equally mixed as indicated in Fig. 2E, resulting in four mixtures. Protein lysates were dissolved in 8 M urea buffer and subjected to tryptic digestion, followed by LC-MS/MS using an Orbitrap-Velos mass spectrometer. MS data were processed by Thermo Proteome Discoverer software for protein quantification and identification. Proteins were filtered by being identified in at two of four replicates ("Count" ≥ 2). There were 1360 proteins identified, among which there are 483 down-regulated and 561 up-regulated upon eIF4A2 KD. Then, these proteins were filtered on the basis of whether their mRNA levels are considered as not changed upon eIF4A2 KD, whether their mRNAs are eIF4A2 targets, and whether their mRNAs are eIF4A2 TIR targets (fig. S3E). All the data and statistical results, including the SD and relative SD (RSD), as well as the filter processes are present in table S2.

Apoptosis detection assay and flow cytometry

Apoptotic analysis was determined using the fluorescein isothiocyanate (FITC) annexin V apoptosis detection kit with propidium iodide (PI) (640914, BioLegend) and performed according to the manufacturer's manual. First, single-cell suspension was achieved using cell strainers to remove large clumps of cells. Then, both annexin V– and PI-stained cells were analyzed by flow cytometry. The flow cytometry used an LSR-II Flow Cytometer (BD Biosciences), and data were analyzed using FlowJo software.

Protein synthesis measurements using *O*-propargyl-puromycin incorporation

O-propargyl-puromycin (OP-puro) is used to label nascent peptides, indicating a global translation level (*66*). To measure protein synthesis, ESCs were incubated for 30 min in serum/LIF medium supplemented with OP-Puro (50 μM; ab146664, Abcam). Cells were then harvested, washed with PBS, fixed with 4% paraformaldehyde for 15 min on ice, and permeabilized with PBS supplemented with 3% FBS for 5 min at room temperature. The Click-iT Plus OP-Puro Alexa Fluor 647 assay was done according to the manufacturer's protocol (Click-iT Cell Reaction Buffer Kit, C10269, Thermo Fisher Scientific). Cells were resuspended in 200 μl of PBS supplemented with 3% FBS and 0.1% saponin and analyzed by flow cytometry. To inhibit OP-Puro incorporation (the CHX group), cycloheximide (CHX; 100 μg/ml) was added 30 min before OP-Puro.

Luciferase assay

Luciferase assay was performed in ESCs transfected with 10 ng of pRL-TK and 200 ng of luciferase reporter plasmids containing the 5′UTR elements using Lipofectamine 3000. Forty-eight hours after transfection, the cells were lysed, and luminescence was assayed using the Dual-Glo luciferase assay kit (E2920, Promega) according to the manufacturer's manual. The measurements were performed in triplicate biological samples.

RNA extraction and quantitative reverse transcription polymerase chain reaction

RNA was extracted from the indicated cell lines with the RNeasy Kit (74136, QIAGEN) and converted to cDNA using qScript (95048, Quanta). Relative gene expression levels were analyzed with Lightcycler 480 SYBR green master mix (4729749001, Roche) on the LightCycler480 real-time polymerase chain reaction (PCR) system (Roche). Gene expression levels were normalized to the β-actin expression level.

RNA-seq and data analysis

RNA-seq was performed in ESCs infected with control shRNAs or eIF4A2 shRNAs. Biological duplicates were prepared. Total RNA from each sample was extracted from the cells with the RNeasy kit (74136, QIAGEN). Samples were prepared, indexed, pooled, and sequenced on the Illumina HiSeq system according to a polyadenylated RNA selection protocol per the manufacturer's instructions.

RNA-seq reads were aligned to the mouse mm9 genome using Bowtie2 (v2.3.4.3), and aligned bam files were sorted by name using the parameter -n. We used the HTSeq software (v0.11.2) and mm9 annotation file from GENCODE (www.gencodegenes.org/mouse/release_M1.html) to count reads for each gene using parameters -r name -f bam, and BioMart (*67*) to retrieve corresponding genes names. Last, read counts were normalized with the trimmed mean of M-values (TMM) method (*68*) for differential expression analysis using edgeR (v3.26.8) (*69*).

Public RNA-seq data were downloaded (refer to Data and materials availability), aligned to mm9, and then followed by the same processing setting as mentioned above. The significance value in Fig. 5G and fig. S8K reflects the probability of finding overlapping genes using the hypergeometric test.

RNA secondary structure prediction

RNA secondary structures were determined using (i) RNAfold web server with minimum free energy prediction and thermodynamic ensemble prediction (http://rna.tbi.univie.ac.at/cgi-bin/RNAWebSuite/RNAfold.cgi); (ii) RNAstructure (https://rna.urmc.rochester.edu/RNAstructureWeb/Servers/Predict1/Predict1.html) with Fold results, MaxExpect results, and ProbKnot results; (iii) vs_subopt (version 5.39) (http://rna.it-chiba.ac.jp/~vsfold/vs_subopt/).

The energy of stem-loop, stack, exterior-loop, and bulge-loop are computed by the software RNAstruture (v6.2) (https://rna.urmc.rochester.edu/RNAstructure.html). For each gene, only the structure with the lowest total energy is taken into consideration.

GO and GSEA

GO analysis was carried out by the DAVID (The Database for Annotation, Visualization, and Integrated Discovery) functional annotation program (https://david.ncifcrf.gov/home.jsp). The terms are ranked according to the *P* value that the program provided with default parameters.

GSEA (v4.1.0, available at www.gsea-msigdb.org/gsea/index.jsp) was used to determine whether the set was statistically enriched in eIF4A2 KD versus control KD, Ddx6 KO versus WT (*38*), and H3.3 KD versus control KD (*8*). The 2C-like ESC (Z4 event–associated) gene set was from a published RNA-seq dataset containing significantly more highly expressed genes in Zscan4$^+$ cells than in Zscan4$^-$ cells (*17*). The other gene sets were from the GSEA MSigDB database (the Molecular Signatures Database): epidermis development (systematic name: M14065), mesoderm development (systematic name: M15421), endoderm differentiation (systematic name: M34153), formation of primary germ layer (systematic name: M10670), placenta genes (systematic name: M16071), hindbrain differentiation (systematic name: M13307), and cell differentiation (GO: 0030154). The normalized enrichment score (NES) and false discovery rate (FDR) were calculated by GSEA and indicated for each enrichment test.

eCLIP-seq and data analysis

eCLIP-seq libraries were performed in duplicates according to the published eCLIP-seq protocol (*20*). Briefly, 20 million ESCs were UV cross-linked at 400 mJ/cm^2 with 254-nm radiation. Cells were lysed in iCLIP lysis buffer and sonicated with Bioruptor. The cell lysates were treated with diluted ribonuclease I (RNase I) to fragment RNA. The eIF4A2 antibody (ab31218, Abcam) was precoupled to Protein G Dynabeads and then added into the cell lysate, followed by overnight incubation at 4°C. A total of 2% of the lysate was taken as the input sample, and the remaining lysate was magnetically separated and washed with lysis buffer. During washing, RNA was dephosphorylated with FastAP and T4 PNK, followed by a 3′RNA adapter ligation with T4 RNA ligase. Then, Protein-RNA complexes were separated by an SDS-PAGE gel and transferred to nitrocellulose membranes. eCLIP was performed by excising the membrane area on the basis of the molecular weight of eIF4A2 from the site of

their molecular weight (47 kDa) to the site with 75 kDa more (122 kDa). The SMInput (size-matched input) was used for each biological replicate, and the excised area was the same as its corresponding IP sample. The details of RNA adapter ligation, IP, Western blot, RNA purification, reverse transcription, DNA adapter ligation, cDNA quantification, PCR amplification, and library purification were performed as eCLIP-seq protocol (*20*).

eCLIP-seq reads were processed by following the Nature Method protocol (*20*). Adapters were trimmed (cutadapt v1.18), and reads less than 18 base pair were discarded using parameters -m 18 -a NNNNNNNNNNAGATCGGAAGAGCACACGTCTGAACTCCAGTCAC -g ACGCTCTTCCGATCT -A AGATCGGAAGAGCGT -A GATCGGAAGAGCGTC -A ATCGGAAGAGCGTCG -A TCGGAAGAGCGTCGT -ACGGAAGAGCGTCGTG -AGGAAGAGCGTCGTGT for round 1 and parameters -m 18 -A AGATCGGAAGAGCGT -A GATCGGAAGAGCGTC -A ATCGGAAGAGCGTCG -A TCGGAAGAGCGTCGT -A CGGAAGAGCGTCGTG -A GGAAGAGCGTCGTGT for round 2. Mapping reads were then performed against mouse elements in RepBase (*70*) with STAR (v2.6.1b) (*71*). Repeat mapping reads were segregated, and all others were mapped against the mouse mm9 genome with STAR (v2.6.1b). PCR duplicates were removed from uniquely mapping reads to get usable reads. Multiple in-line barcodes were merged for usable reads, followed by peak identification with the clipper software (v0.2.0, https://pypi.org/project/clipper/) using parameters -s mm9 --Bonferroni --superlocal --threshold-method binomial --save-pickle on read 2 only (Bonferroni correction was used on our peaks to reduce false positives. A semiexperimental option, "-superlocal" was used to pick up peaks that may be missed with genome-wide or gene-wide thresholds). In addition, on the basis of these candidate peaks, we further use the eCLIP size-matched input as control and then compare eCLIP with the input data to get peaks enriched in eCLIP samples with an intensity fold change of more than two. Given these, we used the same code "-s mm9 --Bonferroni --superlocal --threshold-method binomial --save-pickle" for peak calling and "Peak_input_normalization_wrapper.pl" for peak normalization in the abovementioned Nature Method paper and then filtered with a fold change of >2 to get our peaks. TIRs were extracted by the code (https://github.com/stephenfloor/extract-transcript-regions). Binding peaks on the coding exon and TIR were extracted as the target- and TIR target–binding peaks. These peaks were then annotated with gene names using annotatePeaks.pl script in HOMER tools (*72*), respectively. Genes in the former list were identified as targets, and those in the latter were TIR targets.

For repetitive analysis, both reads were counted for input and eCLIP data on 3′UTR, intron, CDS, and 5′UTR regions and then normalized by the TMM method (*68*). Fold changes were calculated for both replicates using the TMM value. The correlation coefficient was lastly calculated on the basis of fold change values to indicate the data repeatability. For peak distribution analysis, we used the Guitar (v1.20.1) (*73*) to visualize the binding frequency on 5′UTR, CDS, and 3′UTR regions.

Ribosome profiling and data analysis

Ribosome profiling was performed using ESCs infected with control shRNAs (sh*NT* and sh*GFP*) or eIF4A2 shRNAs. Total RNA and RPF libraries were prepared using the TruSeq Ribo Profile (Mammalian) Kit (RPHMR12126, Illumina) according to the manufacturer's reference guide (document no. 15066016 v01) with Ribo-Zero Gold Kit (H/M/R) (MRZG126, Illumina). The prepared libraries were sequenced on a HiSeq 2500 system (Illumina).

Ribosome profiling data reads were first adapter-trimmed using FASTX-Toolkit (v0.0.14; http://hannonlab.cshl.edu/fastx_toolkit) with the parameter -a AGATCGGAAGAGCACACGTCT. Then, ribosomal RNA and transfer RNA reads were removed using Bowtie (v1.2.3). The remaining reads are aligned to the mouse mm9 genome using TopHat (v2.1.1). The matched total RNA-seq data were also processed with the same processing procedure. These aligned bam files were sorted by name with the parameter –n and counted by HTSeq (v0.11.2). For genes, we counted using parameters -r name -f bam. For transcripts, we used parameters -r name -f bam --nonunique all to count reads on TIR and CDS regions. All read counts were normalized using the TMM method (*68*).

In Fig. 3A, to select the candidates through which eIF4A2 controls the translation initiation program to safeguard ESC identity, we applied the following stringent criteria to filter the eIF4A2 targets [from the middle (table S3) to the bottom (table S4) in Fig. 3A]: (i) the mRNAs are targeted by eIF4A2 at TIR; (ii) upon eIF4A2 KD, RPF changes on both TIR and FL RNA have a similar trend (both increase or both decrease); and (iii) the mRNAs with low ribosome density are excluded to obtain the most accurately regulated changes instead of the variance caused by noises [the targets with either of the following conditions were excluded: (i) the average TMM of RPF on FL RNA in all samples <15; (ii) the average TMM of RPF on RNA TIR in all samples/TIR length (in nucleotides) < 0.02]. Notably, the pluripotency-associated targets (fig. S3E) are not in the group of translational change (Fig. 3A, bottom) due to their RPF fold changes at TIRs not crossing the threshold 0.5 (higher than 0.5).

Polysome profiling data analysis

Public polysome profiling data were downloaded [Gene Expression Omnibus (GEO); accession: GSE112761) and then trimmed using Trim Galore (v0.5.0). Trimmed data were aligned to the mm9 genome using bowtie2 (v2.3.4.3) and then sorted with parameter -n and counted using HTSeq software (v0.11.2). All read counts were normalized using the TMM method.

Sequence enrichment analysis

Information for all mm9 mRNA transcripts was extracted from the Ensembl database (Release 67, http://may2012.archive.ensembl.org/Mus_musculus/Info/Index), including 5′UTR length, 5′UTR sequence, CDS length, CDS. The minimum free energy was calculated for all 5′UTR sequences using RNAalifold (v2.4.11) (*74*). We conducted sequence motif analysis on 5′UTR sequences, TIR-binding sequences, and ribosome-binding sequences around the start codon, and these results were visualized by the ggseqlogo (v0.1) (*75*).

Motif enrichment analysis

RNA motifs were determined using the findMotifsGenome.pl script in HOMER tools (*72*) with the parameter -rna.

High-throughput sequencing data visualization

All processed and index-sorted bam files of high-throughput sequencing data were converted to TDF files using the count command of igvtools, followed by visualization using IGV (Integrative Genomics Viewer) software (*76*).

Quantification and statistical analysis

Except for GSEA, all other statistical analysis was performed with GraphPad Prism (GraphPad Software Inc.), Excel, or R (www.r-project.org/). Statistical significance was identified by Student's *t* test or one-way analysis of variance with Tukey's posttest as indicated in the manuscript or figure legends. *P* values of less than 0.05 were considered statistically significant. $*P < 0.05$, $**P < 0.01$, and $***P < 0.001$.

SUPPLEMENTARY MATERIALS

Supplementary material for this article is available at https://science.org/doi/10.1126/sciadv.abm0478

View/request a protocol for this paper from *Bio-protocol*.

REFERENCES AND NOTES

1. T. W. Theunissen, R. Jaenisch, Mechanisms of gene regulation in human embryos and pluripotent stem cells. *Development* **144**, 4496–4509 (2017).
2. D. Li, M. S. Kishta, J. Wang, Regulation of pluripotency and reprogramming by RNA binding proteins. *Curr. Top. Dev. Biol.* **138**, 113–138 (2020).
3. J. A. Hackett, Y. Huang, U. Günesdogan, K. A. Gretarsson, T. Kobayashi, M. A. Surani, Tracing the transitions from pluripotency to germ cell fate with CRISPR screening. *Nat. Commun.* **9**, 4292 (2018).
4. J. A. Saba, K. Liakath-Ali, R. Green, F. M. Watt, Translational control of stem cell function. *Nat. Rev. Mol. Cell Biol.* **22**, 671–690 (2021).
5. T. S. Macfarlan, W. D. Gifford, S. Driscoll, K. Lettieri, H. M. Rowe, D. Bonanomi, A. Firth, O. Singer, D. Trono, S. L. Pfaff, Embryonic stem cell potency fluctuates with endogenous retrovirus activity. *Nature* **487**, 57–63 (2012).
6. H. Niwa, J. I. Miyazaki, A. G. Smith, Quantitative expression of Oct-3/4 defines differentiation, dedifferentiation or self-renewal of ES cells. *Nat. Genet.* **24**, 372–376 (2000).
7. H. Niwa, Y. Toyooka, D. Shimosato, D. Strumpf, K. Takahashi, R. Yagi, J. Rossant, Interaction between Oct3/4 and Cdx2 determines trophectoderm differentiation. *Cell* **123**, 917–929 (2005).
8. L. A. Banaszynski, D. Wen, S. Dewell, S. J. Whitcomb, M. Lin, N. Diaz, S. J. Elsässer, A. Chapgier, A. D. Goldberg, E. Canaani, S. Rafii, D. Zheng, C. D. Allis, Hira-dependent histone H3.3 deposition facilitates PRC2 recruitment at developmental loci in ES cells. *Cell* **155**, 107–120 (2013).
9. C. E. Aitken, J. R. Lorsch, A mechanistic overview of translation initiation in eukaryotes. *Nat. Struct. Mol. Biol.* **19**, 568–576 (2012).
10. Y. Gao, X. Liu, B. Tang, C. Li, Z. Kou, L. Li, W. Liu, Y. Wu, X. Kou, J. Li, Y. Zhao, J. Yin, H. Wang, S. Chen, L. Liao, S. Gao, Protein expression landscape of mouse embryos during pre-implantation development. *Cell Rep.* **21**, 3957–3969 (2017).
11. N. Y. Chia, Y. S. Chan, B. Feng, X. Lu, Y. L. Orlov, D. Moreau, P. Kumar, L. Yang, J. Jiang, M. S. Lau, M. Huss, B. S. Soh, P. Kraus, P. Li, T. Lufkin, B. Lim, N. D. Clarke, F. Bard, H. H. Ng, A genome-wide RNAi screen reveals determinants of human embryonic stem cell identity. *Nature* **468**, 316–320 (2010).
12. H. Sugiyama, K. Takahashi, T. Yamamoto, M. Iwasaki, M. Narita, M. Nakamura, T. A. Rand, M. Nakagawa, A. Watanabe, S. Yamanaka, Nat1 promotes translation of specific proteins that induce differentiation of mouse embryonic stem cells. *Proc. Natl. Acad. Sci. U.S.A.* **114**, 340–345 (2017).
13. T. Hart, M. Chandrashekhar, M. Aregger, Z. Steinhart, K. R. Brown, G. MacLeod, M. Mis, M. Zimmermann, A. Fradet-Turcotte, S. Sun, P. Mero, P. Dirks, S. Sidhu, F. P. Roth, O. S. Rissland, D. Durocher, S. Angers, J. Moffat, High-resolution CRISPR screens reveal fitness genes and genotype-specific cancer liabilities. *Cell* **163**, 1515–1526 (2015).
14. Q. L. Ying, J. Wray, J. Nichols, L. Batlle-Morera, B. Doble, J. Woodgett, P. Cohen, A. Smith, The ground state of embryonic stem cell self-renewal. *Nature* **453**, 519–523 (2008).
15. A. Pause, N. Sonenberg, Mutational analysis of a DEAD box RNA helicase: The mammalian translation initiation factor eIF-4A. *EMBO J.* **11**, 2643–2654 (1992).
16. S. E. Vidal, B. Amlani, T. Chen, A. Tsirigos, M. Stadtfeld, Combinatorial modulation of signaling pathways reveals cell-type-specific requirements for highly efficient and synchronous iPSC reprogramming. *Stem Cell Reports* **3**, 574–584 (2014).
17. T. Akiyama, L. Xin, M. Oda, A. A. Sharov, M. Amano, Y. Piao, J. S. Cadet, D. B. Dudekula, Y. Qian, W. Wang, S. B. H. Ko, M. S. H. Ko, Transient bursts of Zscan4 expression are accompanied by the rapid derepression of heterochromatin in mouse embryonic stem cells. *DNA Res.* **22**, 307–318 (2015).
18. G. Galicia-Vázquez, R. Cencic, F. Robert, A. Q. Agenor, J. Pelletier, A cellular response linking eIF4AI activity to eIF4AII transcription. *RNA* **18**, 1373–1384 (2012).
19. G. Galicia-Vázquez, J. Chu, J. Pelletier, eIF4AII is dispensable for miRNA-mediated gene silencing. *RNA* **21**, 1826–1833 (2015).
20. E. L. Van Nostrand, G. A. Pratt, A. A. Shishkin, C. Gelboin-Burkhart, M. Y. Fang, B. Sundararaman, S. M. Blue, T. B. Nguyen, C. Surka, K. Elkins, R. Stanton, F. Rigo, M. Guttman, G. W. Yeo, Robust transcriptome-wide discovery of RNA-binding protein binding sites with enhanced CLIP (eCLIP). *Nat. Methods* **13** 508–514 (2016).
21. K. Leppek, R. Das, M. Barna, Functional 5′ UTR mRNA structures in eukaryotic translation regulation and how to find them. *Nat. Rev. Mol. Cell Biol.* **19**, 158–174 (2018).
22. W. Zhang, F. Chen, R. Chen, D. Xie, J. Yang, X. Zhao, R. Guo, Y. Zhang, Y. Shen, J. Göke, L. Liu, X. Lu, Zscan4c activates endogenous retrovirus MERVL and cleavage embryo genes. *Nucleic Acids Res.* **47**, 8485–8501 (2019).
23. R. A. Young, Control of the embryonic stem cell state. *Cell* **144**, 940–954 (2011).
24. M. Giacomello, A. Pyakurel, C. Glytsou, L. Scorrano, The cell biology of mitochondrial membrane dynamics. *Nat. Rev. Mol. Cell Biol.* **21**, 204–224 (2020).
25. V. Ding, Q. J. Lew, K. L. Chu, S. Natarajan, V. Rajasegaran, M. Gurumurthy, A. B. H. Choo, S. H. Chao, HEXIM1 induces differentiation of human pluripotent stem cells. *PLOS ONE* **8**, e72823 (2013).
26. S. Mesman, M. P. Smidt, Tcf12 is involved in early cell-fate determination and subset specification of midbrain dopamine neurons. *Front. Mol. Neurosci.* **10**, 353 (2017).
27. J. Wray, T. Kalkan, S. Gomez-Lopez, D. Eckardt, A. Cook, R. Kemler, A. Smith, Inhibition of glycogen synthase kinase-3 alleviates Tcf3 repression of the pluripotency network and increases embryonic stem cell resistance to differentiation. *Nat. Cell Biol.* **13**, 838–845 (2011).
28. L. Cimmino, O. Abdel-Wahab, R. L. Levine, I. Aifantis, TET family proteins and their role in stem cell differentiation and transformation. *Cell Stem Cell* **9**, 193–204 (2011).
29. O. Meyuhas, T. Kahan, The race to decipher the top secrets of TOP mRNAs. *Biochim. Biophys. Acta* **1849**, 801–811 (2015).
30. R. Yamashita, S. Sugano, Y. Suzuki, K. Nakai, DBTSS: DataBase of transcriptional start sites progress report in 2012. *Nucleic Acids Res.* **40**, D150–D154 (2012).
31. C. C. Thoreen, L. Chantranupong, H. R. Keys, T. Wang, N. S. Gray, D. M. Sabatini, A unifying model for mTORC1-mediated regulation of mRNA translation. *Nature* **485**, 109–113 (2012).
32. D. Li, J. Wang, Ribosome heterogeneity in stem cells and development. *J. Cell Biol.* **219**, e202001108 (2020).
33. M. B. Ferretti, H. Ghalei, E. A. Ward, E. L. Potts, K. Karbstein, Rps26 directs mRNA-specific translation by recognition of Kozak sequence elements. *Nat. Struct. Mol. Biol.* **24**, 700–707 (2017).
34. A. P. Hutchins, Z. Yang, Y. Li, F. He, X. Fu, X. Wang, D. Li, K. Liu, J. He, Y. Wang, J. Chen, M. A. Esteban, D. Pei, Models of global gene expression define major domains of cell type and tissue identity. *Nucleic Acids Res.* **45**, 2354–2367 (2017).
35. F. Yang, X. Huang, R. Zang, J. Chen, M. Fidalgo, C. Sanchez-Priego, J. Yang, A. Caichen, F. Ma, T. Macfarlan, H. Wang, S. Gao, H. Zhou, J. Wang, DUX-miR-344-ZMYM2-mediated activation of MERVL LTRs induces a totipotent 2C-like state. *Cell Stem Cell* **26**, 234–250.e7 (2020).
36. G. Falco, S. L. Lee, I. Stanghellini, U. C. Bassey, T. Hamatani, M. S. H. Ko, Zscan4: A novel gene expressed exclusively in late 2-cell embryos and embryonic stem cells. *Dev. Biol.* **307**, 539–550 (2007).
37. A. Wilczynska, S. L. Gillen, T. Schmidt, H. A. Meijer, R. Jukes-Jones, C. Langlais, K. Kopra, W. T. Lu, J. D. Godfrey, B. R. Hawley, K. Hodge, S. Zanivan, K. Cain, J. le Quesne, M. Bushell, eIF4A2 drives repression of translation at initiation by Ccr4-Not through purine-rich motifs in the 5'UTR. *Genome Biol.* **20**, 262 (2019).
38. J. W. Freimer, T. J. Hu, R. Blelloch, Decoupling the impact of microRNAs on translational repression versus RNA degradation in embryonic stem cells. *eLife* **7**, e38014 (2018).
39. B. Di Stefano, E.-C. Luo, C. Haggerty, S. Aigner, J. Charlton, J. Brumbaugh, F. Ji, I. R. Jiménez, K. J. Clowers, A. J. Huebner, K. Clement, I. Lipchina, M. A. C. de Kort, A. Anselmo, J. Pulice, M. F. M. Gerli, H. Gu, S. P. Gygi, R. I. Sadreyev, A. Meissner, G. W. Yeo, K. Hochedlinger, The RNA helicase DDX6 controls cellular plasticity by modulating P-body homeostasis. *Cell Stem Cell* **25**, 622–638.e13 (2019).
40. A. M. Klein, L. Mazutis, I. Akartuna, N. Tallapragada, A. Veres, V. Li, L. Peshkin, D. A. Weitz, M. W. Kirschner, Droplet barcoding for single-cell transcriptomics applied to embryonic stem cells. *Cell* **161**, 1187–1201 (2015).
41. M. G. Carter, C. A. Stagg, G. Falco, T. Yoshikawa, U. C. Bassey, K. Aiba, L. V. Sharova, N. Shaik, M. S. H. Ko, An in situ hybridization-based screen for heterogeneously expressed genes in mouse ES cells. *Gene Expr. Patterns* **8**, 181–198 (2008).
42. C. Chen, X. Zhang, Y. Wang, X. Chen, W. Chen, S. Dan, S. She, W. Hu, J. Dai, J. Hu, Q. Cao, Q. Liu, Y. Huang, B. Qin, B. Kang, Y.-J. Wang, Translational and post-translational control of human naïve versus primed pluripotency. *iScience* **25**, 103645 (2021).
43. S. Das Sharma, J. B. Metz, H. Li, B. D. Hobson, N. Hornstein, D. Sulzer, G. Tang, P. A. Sims, Widespread alterations in translation elongation in the brain of juvenile Fmr1 knockout mice. *Cell Rep.* **26**, 3313–3322.e5 (2019).
44. E. W. Mills, R. Green, Ribosomopathies: There's strength in numbers. *Science* **358**, eaan2755 (2017).
45. N. Lane, W. Martin, The energetics of genome complexity. *Nature* **467**, 929–934 (2010).
46. A. Bulut-Karslioglu, T. A. Macrae, J. A. Oses-Prieto, S. Covarrubias, M. Percharde, G. Ku, A. Diaz, M. T. Mc Manus, A. L. Burlingame, M. Ramalho-Santos, The transcriptionally permissive chromatin state of embryonic stem cells is acutely tuned to translational output. *Cell Stem Cell* **22**, 369–383.e8 (2018).

47. X. Pichon, L. A. Wilson, M. Stoneley, A. Bastide, H. A King, J. Somers, A. E Willis, RNA binding protein/RNA element interactions and the control of translation. *Curr. Protein Pept. Sci.* **13**, 294–304 (2012).
48. S. Juszkiewicz, G. Slodkowicz, Z. Lin, P. Freire-Pritchett, S. Y. Peak-Chew, R. S. Hegde, Ribosome collisions trigger cis-acting feedback inhibition of translation initiation. *eLife* **9**, e60038 (2020).
49. Z. Shi, K. Fujii, K. M. Kovary, N. R. Genuth, H. L. Röst, M. N. Teruel, M. Barna, Heterogeneous ribosomes preferentially translate distinct subpools of mRNAs genome-wide. *Mol. Cell* **67**, 71–83.e7 (2017).
50. W. F. Marzluff, E. J. Wagner, R. J. Duronio, Metabolism and regulation of canonical histone mRNAs: Life without a poly(A) tail. *Nat. Rev. Genet.* **9**, 843–854 (2008).
51. L. Shi, H. Wen, X. Shi, The histone variant H3.3 in transcriptional regulation and human disease. *J. Mol. Biol.* **429**, 1934–1945 (2017).
52. F. Aguilo, F. Zhang, A. Sancho, M. Fidalgo, S. di Cecilia, A. Vashisht, D. F. Lee, C. H. Chen, M. Rengasamy, B. Andino, F. Jahouh, A. Roman, S. R. Krig, R. Wang, W. Zhang, J. A. Wohlschlegel, J. Wang, M. J. Walsh, Coordination of m(6)A mRNA methylation and gene transcription by ZFP217 regulates pluripotency and reprogramming. *Cell Stem Cell* **17**, 689–704 (2015).
53. C. Chazaud, Y. Yamanaka, Lineage specification in the mouse preimplantation embryo. *Development* **143**, 1063–1074 (2016).
54. Q. Tian, X. F. Wang, S. M. Xie, Y. Yin, L. Q. Zhou, H3.3 impedes zygotic transcriptional program activated by Dux. *Biochem. Biophys. Res. Commun.* **522**, 422–427 (2020).
55. A. C. Goldstrohm, T. M. T. Hall, K. M. McKenney, Post-transcriptional regulatory functions of mammalian pumilio proteins. *Trends Genet.* **34**, 972–990 (2018).
56. Y. Chen, A. Boland, D. Kuzuoğlu-Öztürk, P. Bawankar, B. Loh, C. T. Chang, O. Weichenrieder, E. Izaurralde, A DDX6-CNOT1 complex and W-binding pockets in CNOT9 reveal direct links between miRNA target recognition and silencing. *Mol. Cell* **54**, 737–750 (2014).
57. I. I. I. Enwerem, N. D. Elrod, C.-T. Chang, A. Lin, P. Ji, J. A. Bohn, Y. Levdansky, E. J. Wagner, E. Valkov, A. C. Goldstrohm, Human pumilio proteins directly bind the CCR4-NOT deadenylase complex to regulate the transcriptome. *RNA* **27**, 445–464 (2021).
58. N. Ivanova, R. Dobrin, R. Lu, I. Kotenko, J. Levorse, C. DeCoste, X. Schafer, Y. Lun, I. R. Lemischka, Dissecting self-renewal in stem cells with RNA interference. *Nature* **442**, 533–538 (2006).
59. J. Betschinger, J. Nichols, S. Dietmann, P. D. Corrin, P. J. Paddison, A. Smith, Exit from pluripotency is gated by intracellular redistribution of the bHLH transcription factor Tfe3. *Cell* **153**, 335–347 (2013).
60. T. G. Fazzio, J. T. Huff, B. Panning, An RNAi screen of chromatin proteins identifies Tip60-p400 as a regulator of embryonic stem cell identity. *Cell* **134**, 162–174 (2008).
61. C. Schaniel, Y. S. Ang, K. Ratnakumar, C. Cormier, T. James, E. Bernstein, I. R. Lemischka, P. J. Paddison, Smarcc1/Baf155 couples self-renewal gene repression with changes in chromatin structure in mouse embryonic stem cells. *Stem Cells* **27**, 2979–2991 (2009).
62. L. Ding, M. Paszkowski-Rogacz, M. Winzi, D. Chakraborty, M. Theis, S. Singh, G. Ciotta, I. Poser, A. Roguev, W. K. Chu, C. Choudhary, M. Mann, A. F. Stewart, N. Krogan, F. Buchholz, Systems analyses reveal shared and diverse attributes of Oct4 regulation in pluripotent cells. *Cell Syst.* **1**, 141–151 (2015).
63. B. Schwanhäusser, D. Busse, N. Li, G. Dittmar, J. Schuchhardt, J. Wolf, W. Chen, M. Selbach, Global quantification of mammalian gene expression control. *Nature* **473**, 337–342 (2011).
64. A. Saunders, X. Huang, M. Fidalgo, M. H. Reimer Jr., F. Faiola, J. Ding, C. Sánchez-Priego, D. Guallar, C. Sáenz, D. Li, J. Wang, The SIN3A/HDAC corepressor complex functionally cooperates with NANOG to promote pluripotency. *Cell Rep.* **18**, 1713–1726 (2017).
65. D. Mellacheruvu, Z. Wright, A. L. Couzens, J. P. Lambert, N. A. St-Denis, T. Li, Y. V. Miteva, S. Hauri, M. E. Sardiu, T. Y. Low, V. A. Halim, R. D. Bagshaw, N. C. Hubner, A. al-Hakim, A. Bouchard, D. Faubert, D. Fermin, W. H. Dunham, M. Goudreault, Z. Y. Lin, B. G. Badillo, T. Pawson, D. Durocher, B. Coulombe, R. Aebersold, G. Superti-Furga, J. Colinge, A. J. R. Heck, H. Choi, M. Gstaiger, S. Mohammed, I. M. Cristea, K. L. Bennett, M. P. Washburn, B. Raught, R. M. Ewing, A. C. Gingras, A. I. Nesvizhskii, The CRAPome: A contaminant repository for affinity purification-mass spectrometry data. *Nat. Methods* **10**, 730–736 (2013).
66. S. Iwasaki, N. T. Ingolia, The growing toolbox for protein synthesis studies. *Trends Biochem. Sci.* **42**, 612–624 (2017).
67. S. Durinck, Y. Moreau, A. Kasprzyk, S. Davis, B. de Moor, A. Brazma, W. Huber, BioMart and Bioconductor: A powerful link between biological databases and microarray data analysis. *Bioinformatics* **21**, 3439–3440 (2005).
68. M. D. Robinson, A. Oshlack, A scaling normalization method for differential expression analysis of RNA-seq data. *Genome Biol.* **11**, R25–R25 (2010).
69. D. J. McCarthy, Y. Chen, G. K. Smyth, Differential expression analysis of multifactor RNA-seq experiments with respect to biological variation. *Nucleic Acids Res.* **40**, 4288–4297 (2012).
70. W. Bao, K. K. Kojima, O. Kohany, Repbase Update, a database of repetitive elements in eukaryotic genomes. *Mob. DNA* **6**, 11 (2015).
71. A. Dobin, C. A. Davis, F. Schlesinger, J. Drenkow, C. Zaleski, S. Jha, P. Batut, M. Chaisson, T. R. Gingeras, STAR: Ultrafast universal RNA-seq aligner. *Bioinformatics* **29**, 15–21 (2013).
72. S. Heinz, C. Benner, N. Spann, E. Bertolino, Y. C. Lin, P. Laslo, J. X. Cheng, C. Murre, H. Singh, C. K. Glass, Simple combinations of lineage-determining transcription factors prime cis-regulatory elements required for macrophage and B cell identities. *Mol. Cell* **38**, 576–589 (2010).
73. X. Cui, Z. Wei, L. Zhang, H. Liu, L. Sun, S.-W. Zhang, Y. Huang, J. Meng, Guitar: An R/bioconductor package for gene annotation guided transcriptomic analysis of RNA-related genomic features. *Biomed. Res. Int.* **2016**, 8367534 (2016).
74. S. H. Bernhart, I. L. Hofacker, S. Will, A. R. Gruber, P. F. Stadler, RNAalifold: Improved consensus structure prediction for RNA alignments. *BMC Bioinformatics* **9**, 474 (2008).
75. O. Wagih, ggseqlogo: A versatile R package for drawing sequence logos. *Bioinformatics* **33**, 3645–3647 (2017).
76. J. T. Robinson, H. Thorvaldsdóttir, W. Winckler, M. Guttman, E. S. Lander, G. Getz, J. P. Mesirov, Integrative genomics viewer. *Nat. Biotechnol.* **29**, 24–26 (2011).

Acknowledgments: We thank A. K. Hadjantonakis for sharing TSC lines; G. Yeo and E. V. Nostrand for eCLIP-seq technical advice; the ISMMS genomics core facility, NYU Langone's genome technology center, and Illumina Tech Support for technical assistance; J. Gregory for the illustrations (Figs. 1A and 2, B and G), a shared instrumentation grant for the LSR II Flow Cytometer (S10RR027050) to the Columbia Center for Translational Immunology (CCTI) Flow Cytometry Core; and members of the Wang laboratory for discussions. **Funding:** The research in Wang laboratory was supported by NIH (GM129157, HD095938, and HD097268) and NYSTEM (C32583GG and C32569GG). **Author contributions:** D.L. designed, conducted the experiments, and wrote the manuscript. D.L., J.Y., and X.H. performed the data analysis. X.H. and H.Z. provided reagents and experimental support. J.W. conceived, designed, supervised the studies, and wrote and approved the final manuscript. **Competing interests:** The authors declare that they have no competing interests. **Data and materials availability:** The RNA-seq, ribosome sequencing, and eCLIP-seq datasets generated during this study are available at NCBI GEO: GSE150682. Previously published data reanalyzed here are available under accession codes GSE66390, GSE76505, GSE112765, GSE112761, and GSE42154. All other data needed to evaluate the conclusions in the paper are present in the paper and/or the Supplementary Materials.

Submitted 25 August 2021
Accepted 7 February 2022
Published 30 March 2022
10.1126/sciadv.abm0478

ScienceAdvances

eIF4A2 targets developmental potency and histone H3.3 transcripts for translational control of stem cell pluripotency

Dan LiJihong YangXin HuangHongwei ZhouJianlong Wang

Sci. Adv., 8 (13), eabm0478. • DOI: 10.1126/sciadv.abm0478

Science Advances (ISSN) is published by the American Association for the Advancement of Science. 1200 New York Avenue NW, Washington, DC 20005. The title *Science Advances* is a registered trademark of AAAS.